

See discussions, stats, and author profiles for this publication at: <https://www.researchgate.net/publication/51564260>

Thiodiacetate–Manganese Chemistry with N ligands: Unique Control of the Supramolecular Arrangement over the Metal Coordination Mode

ARTICLE *in* CHEMISTRY - A EUROPEAN JOURNAL · SEPTEMBER 2011

Impact Factor: 5.73 · DOI: 10.1002/chem.201100988 · Source: PubMed

CITATIONS

6

READS

24

11 AUTHORS, INCLUDING:



Agustín Galindo

Universidad de Sevilla

124 PUBLICATIONS 1,691 CITATIONS

SEE PROFILE



Eleuterio Alvarez

Spanish National Research Council

287 PUBLICATIONS 4,224 CITATIONS

SEE PROFILE



Patrick Rosa

Institut de Chimie de la matière condensée ...

66 PUBLICATIONS 1,230 CITATIONS

SEE PROFILE



Andrea Caneschi

University of Florence

416 PUBLICATIONS 18,161 CITATIONS

SEE PROFILE

Thiodiacetate–Manganese Chemistry with N ligands: Unique Control of the Supramolecular Arrangement over the Metal Coordination Mode

Abdessamad Grirrane,^[a, b] Antonio Pastor,^[a] Agustín Galindo,^{*,[a]} Eleuterio Álvarez,^[c] Carlo Mealli,^{*,[d]} Andrea Ienco,^[d] Annabella Orlandini,^[d] Patrick Rosa,^[e, f] Andrea Caneschi,^[e] Anne-Laure Barra,^[g] and Javier Fernández Sanz^[h]

Abstract: Compounds based on the Mn–tda unit ($\text{tda} = \text{S}(\text{CH}_2\text{COO})_2^{-2}$) and N co-ligands have been analyzed in terms of structural, spectroscopic, magnetic properties and DFT calculations. The precursors $[\text{Mn}(\text{tda})(\text{H}_2\text{O})]_n$ (**1**) and $[\text{Mn}(\text{tda})(\text{H}_2\text{O})_3] \cdot \text{H}_2\text{O}$ (**2**) have been characterized by powder and X-ray diffraction, respectively. Their derivatives with bipyridyl-type ligands have formulas $[\text{Mn}(\text{tda})(\text{bipy})]_n$ (**3**), $[\{\text{Mn}(\text{N-N})_2(\mu\text{-H}_2\text{O})(\mu\text{-tda})_2\}_n]$ (N–N = 4,4'-Me₂bipy (**4**), 5,5'-Me₂bipy, (**5**)) and $[\text{Mn}(\text{tda})\{\text{MeO}\}_2\text{bipy}\cdot 2\text{H}_2\text{O}]_n$ (**6**). Depending on the presence/position of substituents at bipy, the supramolecular arrangement can affect the metal coordination type. While all the complexes consist of 1D coordination polymers, only **3** has a copper–acetate core with

local trigonal prismatic metal coordination. The presence of substituents in **4–6**, together with water co-ligands, reduces the supramolecular interactions and typical octahedral Mn^{II} ions are observed. The unicity of **3** is also supported by magnetic studies and by DFT calculations, which confirm that the unusual Mn coordination is a consequence of extended noncovalent interactions (π – π stacking) between bipy ligands. Moreover, **3** is an example of broken paradigm for supramolecular chemistry. In fact, the desired stereo-

chemical properties are achieved by using rigid metal building blocks, whereas in **3** the accumulation of weak noncovalent interactions controls the metal geometry. Other N co-ligands have also been reacted with **1** to give the compounds $[\text{Mn}(\text{tda})(\text{phen})]_2 \cdot 6\text{H}_2\text{O}$ (**7**) (phen = 1,10-phenanthroline), $[\text{Mn}(\text{tda})(\text{terpy})]_n$ (**8**) (terpy = 2,2':6,2''-terpyridine), $[\text{Mn}(\text{tda})(\text{pyterpy})]_n$ (**9**) (pyterpy = 4'-(4-pyridyl)-2,2':6,2''-terpyridine), $[\text{Mn}(\text{tda})(\text{tpt})(\text{H}_2\text{O})]_2 \cdot 2\text{H}_2\text{O}$ (**10**) and $[\text{Mn}(\text{tda})(\text{tpt})(\text{H}_2\text{O})]_2 \cdot 2\text{H}_2\text{O}$ (**11**) (tpt = 2,4,6-tris(2-pyridyl)-1,3,5-triazine). Their identified mono-, bi- or polynuclear structures clearly indicate that hydrogen bonding is variously competitive with π – π stacking.

Keywords: manganese • metal–organic frameworks • noncovalent interactions • stacking interactions • thiodiac

[a] Dr. A. Grirrane, Dr. A. Pastor, Prof. Dr. A. Galindo
Departamento de Química Inorgánica
Universidad de Sevilla, Aptdo. 1203
41071 Sevilla (Spain)
Fax: (+34) 954-557-153
E-mail: galindo@us.es

[b] Dr. A. Grirrane
Present address: Instituto de Tecnología Química, CSIC
Universidad Politécnica de Valencia
46022 Valencia (Spain)

[c] Dr. E. Álvarez
Instituto de Investigaciones Químicas
Consejo Superior de Investigaciones Científicas
Universidad de Sevilla, Avda. Américo Vespucio 49
Isla de La Cartuja, 41092 Sevilla (Spain)


[d] Dr. C. Mealli, Dr. A. Ienco, Dr. A. Orlandini
Consiglio Nazionale delle Ricerche
Istituto di Chimica Composti Organometallici
Via Madonna del piano 10, 50019 Sesto Fiorentino, Firenze (Italy)
E-mail: mealli@iccom.cnr.it

[e] Dr. P. Rosa, Dr. A. Caneschi
Dipartimento di Chimica and CNR- INSTM RU of Firenze
Università di Firenze, Via della Lastruccia 3
50019 Sesto Fiorentino (Italy)

[f] Dr. P. Rosa
Present address: CNRS
Université de Bordeaux
ICMCB, 87 avenue du Dr. A. Schweitzer, Pessac, F-33608 (France)

[g] Dr. A.-L. Barra
Laboratoire National des Champs Magnétiques Intenses-CNRS
UJF, BP166, 25 Avenue des Martyrs, 38042 Grenoble Cedex 9
(France)

[h] Prof. Dr. J. F. Sanz
Departamento de Química Física
Universidad de Sevilla, 41071 Sevilla (Spain)

 Supporting information for this article is available on the WWW under <http://dx.doi.org/10.1002/chem.201100988>.

Introduction

The research area devoted to metal coordination polymers has increased enormously in the last decades.^[1] These new materials have the denomination of metal–organic frameworks (MOFs)^[2] or hybrid inorganic–organic compounds^[3] and they are interesting for both the intriguing structural motifs^[4] and the potential magnetic,^[5] porous^[6] and catalytic applications.^[7] Design and controlled syntheses of the extended systems have proved to be crucial for specific tasks of the MOFs.^[8] Control of the network geometry habitually exploits rigid ligands to form primary building blocks with well-known coordination motifs at the metal centres. One of the most widely used ligands in the design of coordination polymers is the versatile carboxylate group^[9] and, in particular, polycarboxylates, which connect multinuclear metal nodes and form robust MOFs.^[10] A more recent approach is the usage of flexible multidentate ligands that permit structural diversity and the development of adaptable materials.^[11]

Within the ample range of polycarboxylates, our group has dedicated much attention to oxydiacetate (oda) and thiodiacetate (tda) molecules with formula $X(\text{CH}_2\text{COO})_2^{2-}$ ($X = \text{O}$ and S , respectively), which may behave as polydentate, flexible and versatile ligands.^[12] Recently, oda has been used in the preparation of MOFs with porous or magnetic properties^[13] and we also illustrated the impact of this ligand on the chemistry of manganese.^[14] Analogously, the behaviour of tda toward the same metal has been investigated and we provide here an exhaustive report on the synthesis and magnetic characterization of several products, which additionally contain polydentate nitrogen co-ligands and occasionally water. Our attention has focused, in particular, on the diverse crystalline environments, which are observed by tuning-up the properties of the various ligands. An initial point to be made is that Mn^{II} has five unpaired electrons in an isotropic d shell, hence the zero-field stabilization energy has no major electronic bias on the mode of coordination. Therefore, the interaction between the ligands can become an important governing factor. In this respect, we have already communicated that 1D polymers of formula $[\text{Mn}(\text{tda})(\text{bipy})]_n$ (**3**) have a trigonal prismatic metal coordination,^[15a] which is different with respect to any other derivative containing variously substituted bipy ligands (pseudo-octahedral metal geometry).^[15b] To our knowledge, this case has remained, at least till very recently,^[16] an unique example of how π – π stacking can control the metal coordination mode. To confirm the point, the paper compares in detail several derivatives obtained from the same Mn–tda precursor and various N co-ligands. All the latter are potentially capable of π – π stacking, but no energetic pattern as that found with bipy is detected. Rather hydrogen bonding is the main packing force in all the other cases.

Results and Discussion

Synthesis and characterization of the coordination polymer $[\text{Mn}(\text{tda})(\text{H}_2\text{O})]_n$ (1**) and compound $[\text{Mn}(\text{tda})(\text{H}_2\text{O})_3] \cdot \text{H}_2\text{O}$ (**2**):** As previously reported,^[15] treatment of an aerobic aqueous solution of MnCl_2 with a 1:1 mixture of Na_2CO_3 and thiodiacetic acid, $\text{S}(\text{CH}_2\text{COOH})_2$, affords, after appropriate workup, colourless microcrystals of polymeric complex $[\text{Mn}(\text{tda})(\text{H}_2\text{O})]_n$ (**1**) in good yields. The IR spectrum of **1** shows the characteristic absorptions of the thiodiacetate ligand,^[17] for instance an intense broad band at 1591 cm^{-1} due to the antisymmetric vibrations of carboxylate, and other peaks associated to the water ligand. The latter absorptions are shifted to 2460 and 2351 cm^{-1} in the deuterated derivative $[\text{Mn}(\text{tda})(\text{D}_2\text{O})]_n$ (see the Experimental Section). The IR spectrum of **1** is identical (see Figure S1 in the Supporting Information) to those of the structurally characterized polymeric complexes $[\text{Cd}(\text{tda})(\text{H}_2\text{O})]_n$ ^[18] and $[\text{Zn}(\text{tda})(\text{H}_2\text{O})]_n$ ^[19] (separately prepared by us by using the same experimental procedure employed in the synthesis of the manganese counterpart). The structure of **1** was confirmed upon solution and refinement from powder diffraction data (Figure 1) and con-

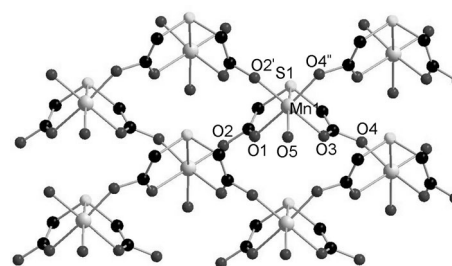


Figure 1. Drawing of the compound $[\text{Mn}(\text{tda})(\text{H}_2\text{O})]_n$ (**1**), which shows the local Mn coordination and the arrangement of the 2D sheet. All hydrogen atoms are omitted for clarity. Symmetry transformations used to generate equivalent atoms: '': $-x-1, y+1/2, -z$; ''': $-x-1, y+1/2, -z+1$.

sists of 2D square layers, in which each metal is pseudo-octahedrally coordinated. In fact each tda ligand acts as tridentate toward one metal by adopting the typical *fac* coordination,^[12] but at the same time the other two oxygen atoms of the carboxylate groups are bound to other two equivalent metal atoms. The tda ligand adopts the bonding mode $\mu_3\text{-}\kappa^3\text{-(O,S,O')},\kappa^1(\text{O'')},\kappa^1(\text{O'''})$, thus involving all of the five donor atoms. One water molecule (*trans* to the S atom) completes the coordination at each metal. The bond of manganese to the thioetheral S atom is rather large $2.689(3)\text{ \AA}$ (the mean value of Mn–S bond lengths is $2.407(4)\text{ \AA}$, as ascertained from a search in the Cambridge Structural Database^[20]), whereas the five Mn–O bonds are in the range $2.083(6)$ – $2.235(6)\text{ \AA}$. Other structural parameters have been collected in Table 1.

The crystallization of **1** occurs from a water solution upon the addition of acetone. On neglecting the latter operation, a second type of colourless block-shaped crystals, **2**, are found mixed with **1**. A slow crystallization from the reaction

Table 1. Selected bond distances [\AA] and angles [$^\circ$] for **1** and **2**.

	1 ^[a]		2
Mn1–O1	2.260(6)	Mn1–O1	2.1167(7)
Mn1–O2	2.129(5)	Mn1–O3	2.1685(6)
Mn1–O3#1	2.235(5)	Mn1–O5	2.1841(7)
Mn1–O4	2.083(6)	Mn1–O6	2.1300(7)
Mn1–O5#2	2.218(6)	Mn1–O7	2.1092(7)
Mn1–S1	2.6886(26)	Mn1–S1	2.7224(3)
O1–Mn1–O2#1	89.9(2)	O1–Mn1–O3	93.48(3)
O1–Mn1–O3	91.9(2)	O1–Mn1–O5	94.29(3)
O1–Mn1–O4#2	170.1(2)	O1–Mn1–O6	90.78(3)
O1–Mn1–O5	88.7(2)	O1–Mn1–O7	168.32(3)
O1–Mn1–S1	78.4(2)	O1–Mn1–S1	77.129(19)
O2#1–Mn1–O3	178.1(2)	O3–Mn1–O5	163.40(3)
O2#1–Mn1–O4#2	87.0(2)	O3–Mn1–O6	95.41(3)
O2#1–Mn1–O5	94.2(2)	O3–Mn1–O7	85.21(3)
O2#1–Mn1–S1	99.5(1)	O3–Mn1–S1	74.941(18)
O3–Mn1–O4#2	98.8(2)	O5–Mn1–O6	99.12(3)
O3–Mn1–O5	87.4(2)	O5–Mn1–O7	84.21(3)
O3–Mn1–S1	78.7(2)	O5–Mn1–S1	92.55(2)
O4#2–Mn1–O5	101.1(2)	O6–Mn1–O7	100.90(3)
O4#2–Mn1–S1	92.1(2)	O6–Mn1–S1	163.82(2)
O5–Mn1–S1	161.4(2)	O7–Mn1–S1	91.34(2)

[a] Symmetry transformations used to generate equivalent atoms: #1: $-x-1, y+1/2, -z$; #2: $-x-1, y+1/2, -z+1$.

mixture, exposed to air, allows the isolation of compound **2** as the major product. The compounds **1** and **2** can be alternatively obtained from each other. Thus **1** forms upon quick crystallization, after the addition of acetone to a water solution of **2**. Conversely, **2** forms from a water solution of **1** upon slow crystallization. The IR spectrum of **2** shows only a few differences with respect to that of **1** but X-ray crystallography allows formulating **2** as the monomeric complex $[\text{Mn}(\text{tda})(\text{H}_2\text{O})_3]\cdot\text{H}_2\text{O}$, which contains a water molecule of co-crystallization besides the three metal coordinated ones. The local metal geometry is again pseudo-octahedral (Figure 2) with tda adopting the same facial coordination mode as in **1** and three additional coordinated H_2O molecules. The Mn–S distance is again long, 2.7224(3) \AA ,^[20] whereas the mean Mn–O bond length is 2.143(1) for tda and 2.141(1) \AA for water. Other structural parameters are collected in Table 1. Compound **2** is isomorphous with the series of complexes $[\text{M}(\text{tda})(\text{H}_2\text{O})_3]\cdot\text{H}_2\text{O}$ (M = Ni,^[21] Zn^[22] and Mg^[23]). In particular, we have previously shown that zinc is also able to form a pair of species similar to **1** and

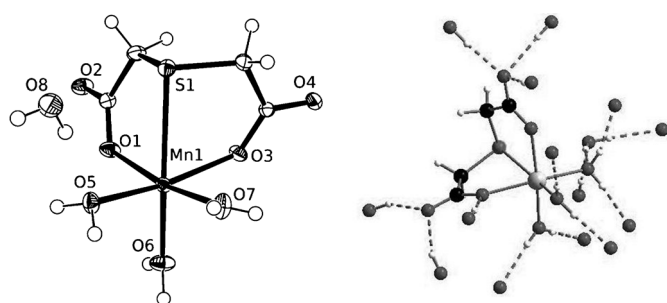
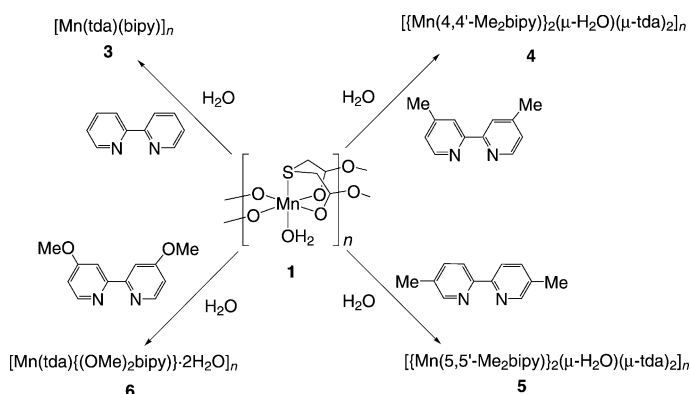


Figure 2. Molecular structure of complex $[\text{Mn}(\text{tda})(\text{H}_2\text{O})_3]\cdot\text{H}_2\text{O}$ (**2**) (left) and the hydrogen network responsible for the 3D pattern (right).

2.^[24] Although the structure of **2** is monomeric, hydrogen bonding involving the external and the coordinated H_2O molecules determines an overall 3D pattern (see Figure 2 and Figure S2 in the Supporting Information).

Reactivity of $[\text{Mn}(\text{tda})(\text{H}_2\text{O})_n]$ (1**) toward bipy N-donor chelates: The role of non-covalent interactions in the assembly of coordination polymers and the control of Mn geometry:** We start presenting the products of the reaction of **1**, in aqueous solution, with unsubstituted or substituted bipyridines, because surprisingly different structural features have been detected.^[15b] The ligands 2,2'-bipyridine (bipy), 4,4'-dimethyl-2,2'-bipyridine (4,4'-Me₂bipy), 5,5'-dimethyl-2,2'-bipyridine (5,5'-Me₂bipy) and 4,4'-dimethoxy-2,2'-bipyridine ((MeO)₂bipy) give rise to the following compounds $[\text{Mn}(\text{tda})(\text{bipy})]_n$ (**3**),^[15a] $[\text{Mn}(\text{N-N})_2(\mu\text{-H}_2\text{O})(\mu\text{-tda})_2]_n$ (N-N = 4,4'-Me₂bipy (**4**); 5,5'-Me₂bipy (**5**))^[15b] and the previously unreported $[\text{Mn}(\text{tda})\{(\text{MeO})_2\text{bipy}\}\cdot 2\text{H}_2\text{O}]_n$ (**6**), respectively. Scheme 1 summarizes ligands and reactions. All products,



Scheme 1. Various products obtained from **1** with ligands containing the bipy skeleton.

isolated in good yields as crystalline solids, are soluble in water but not in low polarity solvents. They are air stable both in solution and in the solid state. The IR spectra are characterized by the absorptions due to the N-donor co-ligands and other broad peaks, corresponding to the tda carboxylate group. X-ray diffraction methods show that all the products are coordination polymers.

As reported before, the structure of **3** consists of 1D ribbons (Figure 3) with bimetallic units being linked through the $-\text{CH}_2\text{SCH}_2-$ chains of two different tda ligands. Therefore, each carboxylate group acts as a bridging bidentate-bimetallic toward two facing Mn^{II} ions and tda adopts the unprecedented bonding mode $\mu, \mu' - \kappa^1(\text{O}), \kappa^1(\text{O}'), \kappa^1(\text{O}'), \kappa^1(\text{O}''')$. Each Mn_2O_8 unit has the dicopper–acetate core, which till recently^[15,25] was unknown in the otherwise rich Mn–carboxylate chemistry.^[26] In view of the orientation of the bipy ligands (uniquely parallel throughout the crystal), each Mn^{II} ion adapts to a local trigonal prismatic coordination, two polyhedra being joined through two rectangular faces at each bimetallic unit.^[27] In contrast, most copper–acetate

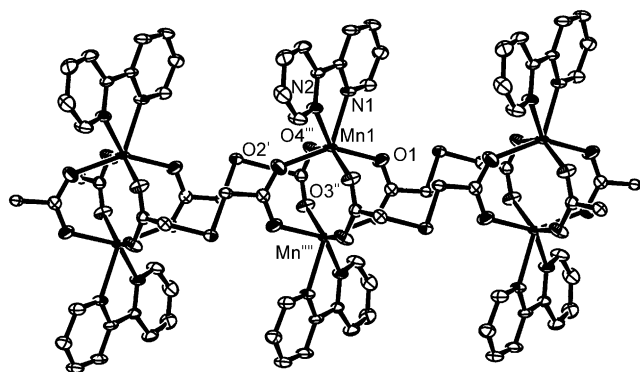


Figure 3. Polymeric chain along the *a* axis of the complex $[\text{Mn}(\text{tda})(\text{bipy})]_n$ (**3**). The hydrogen atoms have been omitted for clarity. Symmetry transformations used to generate equivalent atoms: ' : $-x+1, -y+1, -z$; '' : $-x, -y+1, -z$; ''' : $x+1, y, z$; '''' : $-x+1, -y+1, -z$.

cores correspond either to two square pyramids joined through the bases (when two monodentate axial ligands are present) or two facing squares (in the absence of other co-ligands).^[20] Occasionally, a mixture of the latter situations is observed.^[20]

The average Mn–O and Mn–N bond lengths are 2.162(3) and 2.311(2) Å, respectively, whereas Mn–Mn bonding is excluded by the large distance of 3.502(1) Å. Additional structural parameters are available in Table S1 in the Supporting Information. The covalent 1D ribbons in **3** are threaded into 2D sheets due to supramolecular non-covalent interactions (see Figure S3 in the Supporting Information). As shown in Figure 4, in between any two equally oriented bipy chelates (as van der Waals surfaces) of two consecutive Mn_2 units, another chelate from an adjacent ribbon is inserted upside-down. In such a gear-like compact arrangement, the π – π interactions seem to play a decisive cementing role in spite of the relatively large separation between the planes (ca. 4 Å).^[28] At such a large distance, dispersion van der Waal forces may not be large but they cooperatively provide an overall stabilization to the crystal engineering of the compound. Indeed, the structural pattern of **3** appears unique, since even the smallest substituents at the bipy ligands destroy its compactness upon change of the metal coordination.^[15b]

The compounds **4–6** were indeed synthesized to evaluate the relations between the geometry of the building blocks and the nature of the supramolecular arrangement. To avoid any bias in the synthesis of the derivatives, we adopted reaction conditions most similar to those of **3**. Care was taken that the introduced substituents were symmetrically placed and non-adjacent to the nitrogen atoms to avoid any bias in their dative capabilities. The compounds **4–6** indeed maintain the 1D polymeric structure with 1:1:1 ratio between the components Mn, tda, and N chelate but have evidently lost the high degree of compactness in the 2D sheets. When two relatively small methyl groups occupy the 4,4' or 5,5'-positions of bipy, the corresponding structures **4** and **5** (see Figure 5 and Figure S4, respectively, and their structural parameters in Table S2 in the Supporting Information) are es-

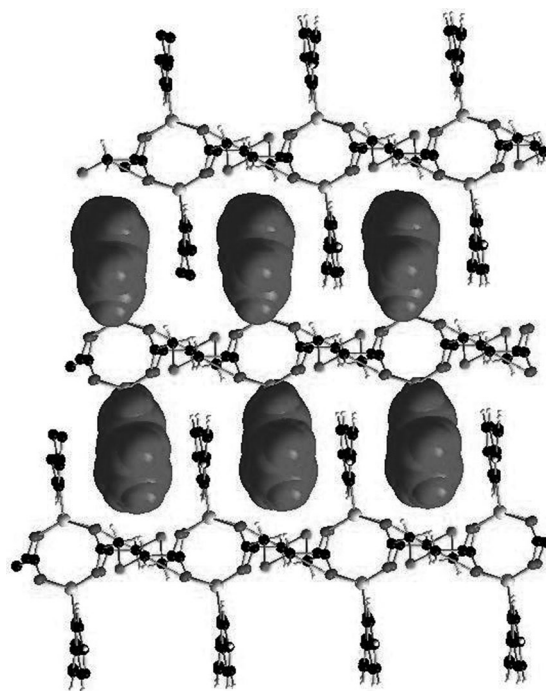


Figure 4. A 2D sheet in the structure of **3**, for which the compact head to tail interpenetration of the parallel bipy ligands belonging to different covalent ribbons is highlighted (as van der Waals surfaces in one ribbon). See colour version of this figure in the Supporting Information.

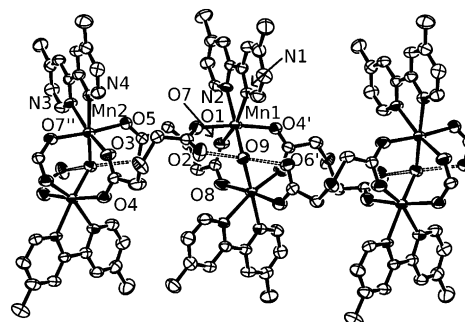


Figure 5. View of the compound $[[\text{Mn}(4,4'\text{-Me}_2\text{bipy})]_2(\mu\text{-H}_2\text{O})(\mu\text{-tda})]_n$ (**4**). The hydrogen atoms are omitted for clarity. The hydrogen bonds between the coordinated H_2O molecule and uncoordinated O atoms of tda are highlighted by dashed lines. Symmetry transformations used to generate equivalent atoms: ' : $-x+1/2, y+1/2, -z+1/2$; '' : $-x+1/2, y-1/2, -z+1/2$.

entially similar to each other, though not isomorphic. As in **3**, the Mn_2 units are interconnected by two tda chains, the S atoms of which are uncoordinated, but the copper acetate core is lost. Only two carboxylate groups continue to act as bidentate–bimetallic, whereas the other two are monodentate and dative only to a different metal atom. Therefore, the ligand tda adopts the bridging mode $\mu_3\text{-}\kappa^1(\text{O}), \kappa^1(\text{O}'), \kappa^1(\text{O}'')$.

Importantly, the local coordination of the metals is no more prismatic but pseudo-octahedral upon the coordination of H_2O as a bridge. In fact, the four oxygen donors to each metal are no more coplanar and, to complete the octa-

hedron in each dimer, the two substituted bipy ligands must become almost perpendicular to each other (in **4** the dihedral angle between the ligands is 72.5°). The bridging H₂O molecule is involved in strong hydrogen bonding with the uncoordinated oxygen atoms of the monodentate carboxylates (the contacts O2...O9 and O6'...O9 are in **4** as short as 2.547(5) and 2.561(5) Å, respectively). This extra source of stability was not present in the water-free compound **3**, the structure of which is evidently favoured by compensating supramolecular interactions. Dimeric species with the core of **4** and **5** are known for other divalent metal ions^[20] and have the general formula [L₂(η¹-OOCR)M]₂(μ-OOCR)₂(μ-H₂O) (L₂=two monodentate N-donor ligands or a bidentate one). Amongst the latter, there are other various Mn^{II} examples,^[29] one of which also contains 4,4'-Me₂bipy^[29b] and has been proposed as a model for the active site of manganese enzymes.^[30]

A relatively good supramolecular organization is attainable by bipy-type ligands,^[31a] as also indicated by other authors who studied Ag complexes with the same N-N ligand as in **4**.^[31b] However, a comparison between **3** and **4** shows that the π-π interactions in the former have a definitely higher degree of compactness. This becomes clearer from Figure 6 which shows (as van der Waals surfaces), the substituted and quasi-orthogonal bipy ligands at the right and left sides of the central ribbon in **4**. The two series consist of planes, which are skewed by about ±45° with respect to the direction of the central ribbon. The bipy molecules of the adjacent ribbons (shown as balls and sticks) still interpenetrate in head-to-tail fashion between any pair of consecutive ligands at the central ribbon, in a pairwise fashion (the separation between planes are not all equivalent). Importantly, the 45° skewing of the aromatic planes with respect to the stacking direction does not permit the quasi-optimal eclipsing of the stacking aromatic ligands.

Figure 7 clearly highlights the differences between **3** and **4**, by showing top-down views of three consecutive bipy ligands in two cases. Whereas almost perfect eclipsing occurs in **3**, the third chelate in **4** is misaligned with respect to the first two that are crystallographically parallel. Additionally, the plane of the third ligand is tilted with respect to the others by ~10°. Therefore, each chelate establishes only one monofacial π-π interaction with its neighbour one, whereas the cumulative stacking observed in **3** is here impossible. The larger compactness of the supramolecular arrangement of **3** versus **4** and **5** is also quantified by a greater crystal density (1.705 vs. 1.540 and 1.520 g cm⁻³, respectively) irrespective of the about 10% larger molecular weight of the bipy substituted compounds. The non-covalent interactions, “the glue of supramolecular chemistry”,^[32a] are very important in directing the self-assembly of coordination compounds. For instance, the effects of non-covalent interactions on controlling coordination geometry,^[16,32b] the coordination mode of the ligand^[32c-e] and the competition between interactions^[32f] and also between the coordination bond and non-covalent interactions^[32g] were published. However, **3** is a unique example, in which the accumulation of π-π stacking

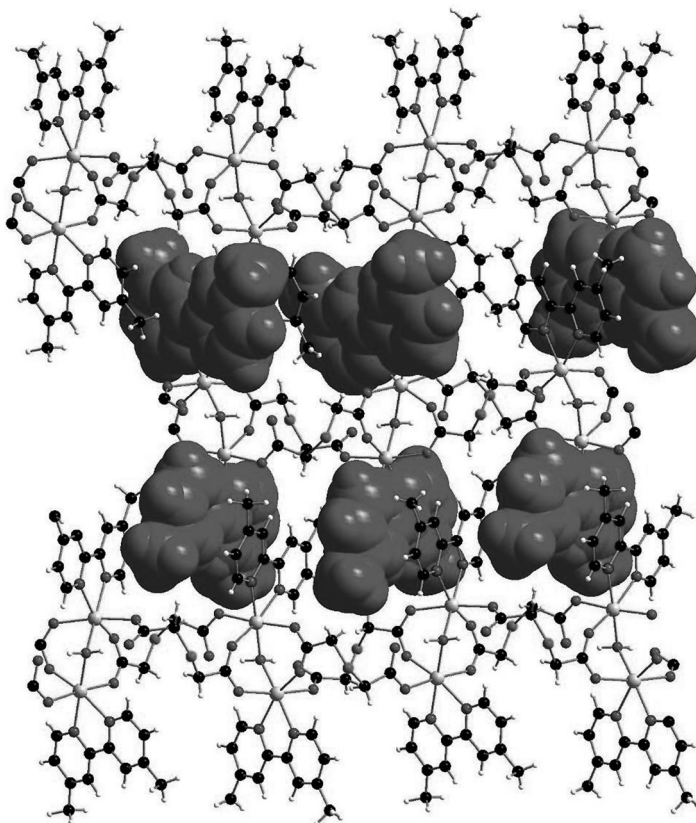


Figure 6. Drawing of one 2D supramolecular sheet in **4** (analogous to that in **5**). The vdW surfaces, at the sides of the central ribbon of Mn₂ units, highlight two sequences of the 4,4'-substituted bipy ligands, which are skewed ~ ±45° with respect to the plane of the sheet. See colour version of this figure in the Supporting Information.

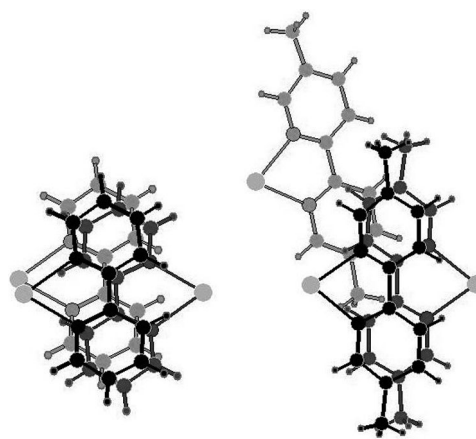


Figure 7. Perpendicular projections in **3** and **4** (left and right side, respectively) of three consecutive bipy skeletons.

uniquely controls the coordination environment of the metal centre.

We synthesized a new compound **6** that contains the even more space-demanding methoxy substituents at the symmetric 4,4'-positions of bipy and in which π-π stacking seems to be definitely lost. The formula of **6**, that is, [Mn(tda)-{(MeO)₂bipy}·2H₂O]_n, matches that of **3** (except for the sol-

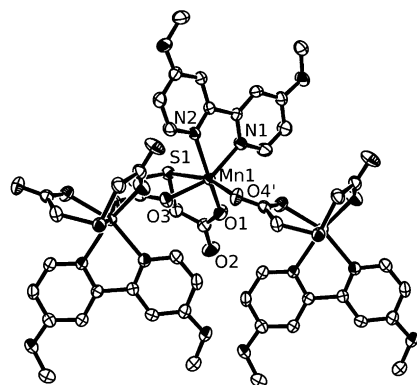


Figure 8. Three mononuclear units forming the 1D ribbons of $[\text{Mn}(\text{tda})\{-\{(\text{MeO})_2\text{bipy}\}\cdot 2\text{H}_2\text{O}\}]_n$ (**6**). Solvent water molecules and hydrogen atoms are omitted for clarity. Symmetry transformations used to generate equivalent atoms: $'$: $-x+3/2, y+1/2, -z+3/2$.

vent water molecules), but the building blocks of the still present 1D ribbons is mononuclear rather than binuclear (see Figure 8 and Figure S5 in the Supporting Information). The local metal coordination is distorted octahedral and consists of the N atoms of one $(\text{MeO})_2\text{bipy}$ chelate, three donors from one tda ligand (*fac*-coordination regardless the large M–S distance of 2.811(1) Å) and one oxygen atom from the next tda ligand. Since one oxygen atom of each tda remains uncoordinated, the ligand's bonding mode is μ_2 - κ^3 -(*O,S,O'*), κ^1 (*O''*). The 1D polymer extends along the cell's *b* axis. In **6**, no 2D pattern occurs through π – π stacking but a layered structure is still possible thanks to the hydrogen-bonding network that involves the H_2O molecules and the uncoordinated oxygen atoms of tda (see Figure S6 in the Supporting Information). The drawing in Figure 9 (only NCCN chelating fragments of bipy are shown) highlights almost planar hexagons formed by uncoordinated oxygen atoms of tda and water molecules and connecting 1D ribbons. The O...O separations are in between 2.7 and 2.9 Å, whereas other geometric details are given in Table 2.

Theoretical studies on models of the compounds **3** and **4–5**:

To gain some theoretical evidence that the supramolecular arrangement in **3** is associated to a unique electronic picture, we performed comparative DFT calculations for models of the binuclear building blocks in **3** and **4** or **5**. Thus, an unit $[\text{Mn}_2(\mu\text{-OOCH})_4(\text{bipy})_2]$ was first optimized (spin multiplicity of 11) in D_{2h} symmetry (model **3a** in Figure 10). The geometric parameters (see Table S3 in the Supporting Information) are satisfactorily similar to those of the single trigonal prisms in **3**, but imaginary frequencies (for the attempted reorientations of the carboxylate and bipy ligands), exclude **3a** as a real minimum. Removal of the symmetry constraints leads to the actual minimum structure, **3b** (Figure 10).

The Mn_2O_8 unit has lost the fourfold symmetry typical of the copper–acetate core, since the *trans* O–Mn–O angles at each metal have assumed the quite different values of 127 and 166°, with the latter almost approaching linearity. At the same time, the two six-membered rings within each bipy

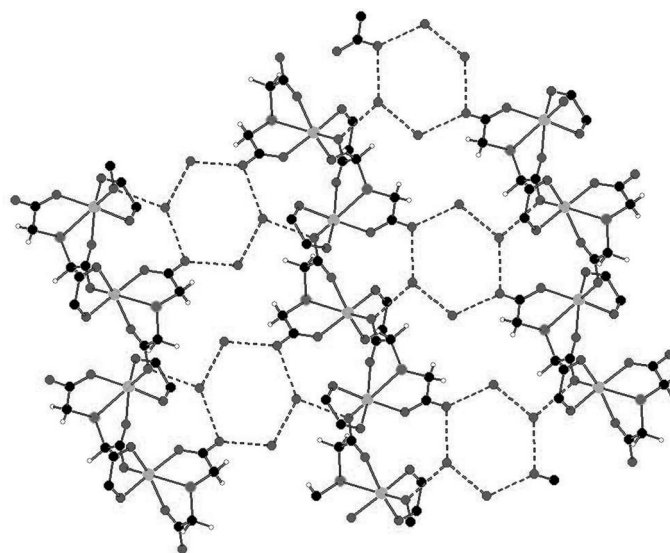


Figure 9. The dimensional pattern of **6** made through hydrogen-bonding interactions. Only the NCCN fragment of the bipy chelates is shown for the sake of clarity. The O...O separations are O2–O7: 2.731(4), O2–O8': 2.919(5), O7–O8'': 2.793(5) Å. Symmetry code: $'$: $x, y+1, z$; $''$: $-x+1, -y, -z+2$. See colour version of this figure in the Supporting Information.

Table 2. Selected bond distances [Å] and angles [°] for **6**.^[a]

Mn1–O1	2.077(3)	Mn1–N1	2.222(3)
Mn1–O3	2.163(2)	Mn1–N2	2.247(3)
Mn1–O4#1	2.129(3)	Mn1–S1	2.8112(11)
O1–Mn1–O3	96.55(11)	O3–Mn1–O4#1	94.67(10)
O1–Mn1–O4#1	97.01(10)	O3–Mn1–N1	157.63(11)
O1–Mn1–N1	96.63(12)	O3–Mn1–N2	89.54(10)
O1–Mn1–N2	162.20(11)	O3–Mn1–S1	73.28(7)
O1–Mn1–S1	74.09(8)	N1–Mn1–N2	72.87(11)
O4#1–Mn1–N1	101.56(11)	N1–Mn1–S1	93.14(9)
O4#1–Mn1–N2	99.15(10)	N2–Mn1–S1	91.84(8)
O4#1–Mn1–S1	163.70(8)	C3–S1–C2	102.1(2)

[a] Symmetry transformations used to generate equivalent atoms: #1: $-x+3/2, y+1/2, -z+3/2$.

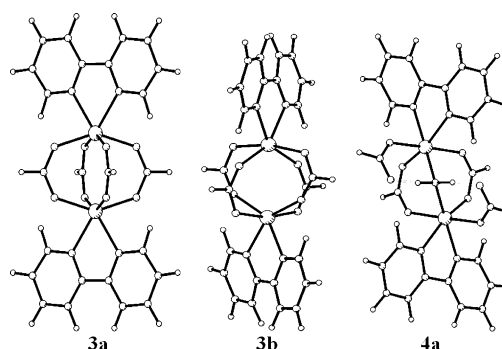


Figure 10. Optimized structures of the models **3a**, **3b** and **4a**.

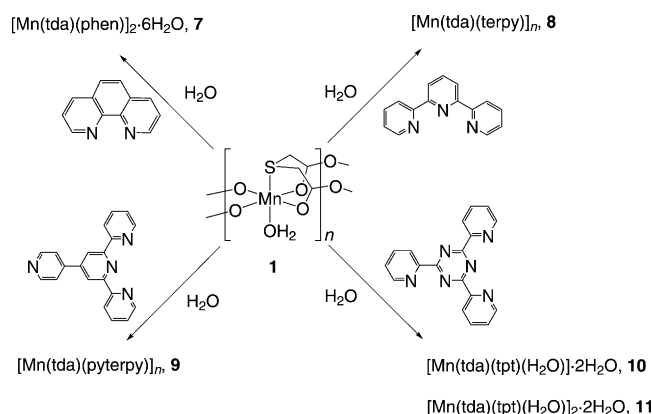
ligand significantly distorted from coplanarity (dihedral angle $\sim 66^\circ$). Therefore, the geometry of the metals is clearly biased toward an octahedron. The model **3b** is more stable than **3a** by only 1.2 kcal mol^{−1}, a result which is consistent with a quasi zero crystal field stabilization energy of d^5 high-

spin metals. Other DFT calculations for the monomeric species $[\text{Mn}(\text{acac})_2(\text{bipy})]^{[33]}$ also showed only a minor energy difference between octahedral and trigonal prismatic coordinations.

Then, we switched to a model of the complexes **4** or **5**, which contain a bridging H_2O molecule, namely $[\text{Mn}_2(\text{bipy})_2(\text{OOCH})_2(\mu\text{-OOCH})_2(\mu\text{-H}_2\text{O})]$ (**4a**). No methyl substituent was introduced at bipy to have fully comparable models. The minimum structure satisfactorily reproduces (see Table S3 in Supporting Information) the stereochemistry and geometry of the binuclear building block of **4** or **5**, in which the two planar bipy ligands are quasi-orthogonal to each other (84°). Importantly, the energy of **4a** is lower by as much as $20.4 \text{ kcal mol}^{-1}$ with respect to the sum of the separated molecules **3a** + H_2O . Such a larger stability of the gas phase can be attributed to the intramolecular hydrogen bonding between the water bridge and the uncoordinated oxygen atoms of the carboxylate groups (see Figures 5 and 10 and Figure S4 in the Supporting Information). For this isolated gas-phase model, evidently the entropy factors are not sufficient to support water dissociation and the stabilization of model **3b**. This is instead possible, in the crystal environment of **3** due to the π - π interactions. These appear singularly negligible (also in view of the large interplanar separations) but, cumulatively, the $\sim 20 \text{ kcal mol}^{-1}$ energy preference of **4a** versus **3a** can be overturned. Although a DFT approach to mimic the actual crystalline environments has not been attempted, we believe that the illustrated computational results sufficiently highlight the importance of the stacking interactions in these systems.

Reactivity of $[\text{Mn}(\text{tda})(\text{H}_2\text{O})]_n$ (1**) toward other bi- or polydentate aromatic N ligands: Synthesis and structural properties:** Comparison of the features of the Mn-tda adducts with unsubstituted or substituted bipy molecules have highlighted the importance of the stacking interactions and their potential function on controlling the metal geometry. At this point, we extended the investigation to the behaviour of the Mn-tda adduct toward nitrogen co-ligands with multiple aromatic N-six-membered rings (either condensate or not), since, in principle, their larger surfaces can further favour π - π stacking. Scheme 2 lists the different reactions with the precursor **1** and the corresponding products.

The first reaction is with 1,10-phenanthroline, which is bidentate similar to bipy, but gives a different product with respect to **3-6**. In fact, $[\text{Mn}(\text{tda})(\text{phen})]_2 \cdot 6\text{H}_2\text{O}$ (**7**) is basically a dimer with the Mn_2O_2 core (Figure 11). In the latter, the bridges are two carboxylate oxygen atoms of two different tda ligands. Each tda adopts the classic *fac* binding mode by using one sulfur and two oxygen atoms (one of which is bridging). The other two oxygen atoms remain uncoordinated but are hydrogen bonded to cocrystallized water molecules. Again, the Mn-S distance is quite long ($2.7588(19) \text{ \AA}$). Local octahedral coordination at the two metals is completed by centrosymmetrically arranged phen chelates, which are π - π stacked in the crystal in directions parallel to the *c* axis (discussed below). Table 3 collects



Scheme 2. Reactions of **1** with other bi- or polydentate aromatic N ligands containing condensed or independent pyridine rings.

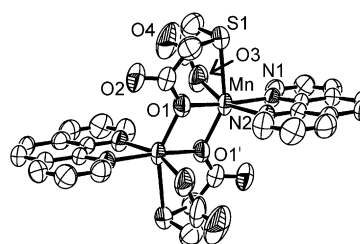


Figure 11. Structure of one discrete dimeric unit in compound $[\text{Mn}(\text{tda})(\text{phen})]_2 \cdot 6\text{H}_2\text{O}$ (**7**). Solvent water molecules and hydrogen atoms are omitted for clarity.

Table 3. Selected bond distances [\AA] and angles [$^\circ$] for **7**.^[a]

Mn1–O1	2.116(3)	Mn1–N1	2.220(3)
Mn1–O1#1	2.193(3)	Mn1–N2	2.223(3)
Mn1–O3	2.086(4)	Mn1–S1	2.759(20)
O1–Mn1–O1#1	76.08(13)	O1#1–Mn1–O3	94.30(14)
O1–Mn1–O3	94.49(15)	O1#1–Mn1–N1	168.17(12)
O1–Mn1–N1	113.35(12)	O1#1–Mn1–N2	96.19(13)
O1–Mn1–N2	105.22(14)	O1#1–Mn1–S1	74.80(12)
O1–Mn1–S1#1	148.40(9)	N1–Mn1–N2	74.80(12)
O3–Mn1–N1	92.09(14)	N1–Mn1–S1	97.17(10)
O3–Mn1–N2	159.40(14)	N2–Mn1–S1	89.99(11)
O3–Mn1–S1	75.70(13)	C3–S1–C2	101.1(3)

[a] Symmetry transformations used to generate equivalent atoms: #1: $-x+3/2, -y+1/2, -z+1$.

structural data, which are consistent with other similar Mn-tda-phen compounds.^[34] Binuclear compound **7** is also isomorphous with the analogous zinc species^[24] and well compares with the compounds $[\text{Cu}(\text{tda})(\text{phen})]_2 \cdot \text{H}_2\text{tda}$ ^[35] and $[\text{Ni}(\text{tda})(\text{en})]_2 \cdot 4\text{H}_2\text{O}$ (en = ethylenediamine).^[36]

The top-down view of Figure 12 highlights four different dimers centred at the corners of a rectangle. In the centre, the projected phen ligands from the four Mn_2 complexes stack together forming one column. The other phen ligands of the four dimers still lie in parallel planes beyond the corners of the rectangle. Each one of them is able to pack with those from adjacent molecules to form four different columns around the central one, although only the seeding

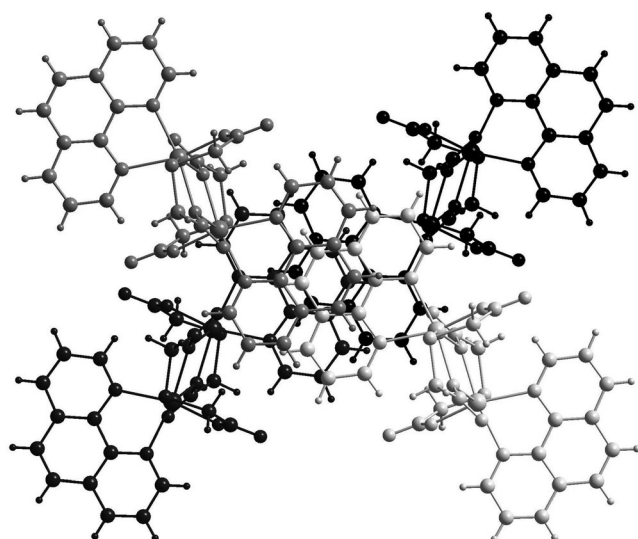


Figure 12. View down the *c* axis to highlight the face-centred columnar arrangement of the phenanthroline ligands in the crystal of $[\text{Mn}(\text{tda})(\text{phen})]_2 \cdot 6\text{H}_2\text{O}$ (**7**). See colour version of this figure in the Supporting Information.

rings appear in Figure 12. Another four neighbour columns (not shown) form in the extended pattern channels, which are occupied by water molecules, hydrogen-bonded with the tda uncoordinated oxygen atoms (see Figures S7 and S8 in the Supporting Information). Altogether, the crystal adopts a 3D pattern because, beside the direction defined by the π – π stacking, the columns are interconnected in the other two directions by the Mn_2O_2 rings. Interestingly, the water molecules can be removed from the channels by heating the crystal at 45 °C for several hours.

Another three different polydentate nitrogen ligands were then reacted with **1**, namely 2,2':6,2''-terpyridine (terpy), 4'-(4-pyridyl)-2,2':6,2''-terpyridine (pyterpy) and 2,4,6-tris(2-pyridyl)-1,3,5-triazine (tpt) (see Scheme 2). The compounds $[\text{Mn}(\text{tda})(\text{terpy})]_n$ (**8**), $[\text{Mn}(\text{tda})(\text{pyterpy})]_n$ (**9**), $[\text{Mn}(\text{tda})(\text{tpt})(\text{H}_2\text{O})]_2 \cdot 2\text{H}_2\text{O}$ (**10**) and $[\text{Mn}(\text{tda})(\text{tpt})(\text{H}_2\text{O})]_2 \cdot 2\text{H}_2\text{O}$ (**11**), respectively, were isolated in good yields. These compounds are air stable in the solid state and display IR spectra with broad absorptions corresponding to the tda carboxylate groups and additional bands due to the respective N-donor co-ligands. The products **8** and **9** are yellow solids, which are insoluble in organic solvents and only barely in water. Due to the absence of water absorptions in the IR spectra and on the basis of analytical data, the compounds are most likely polymeric analogues of the copper species $[\text{Cu}(\text{tda})(\text{terpy})]_n$.^[37] In fact the IR spectrum of the latter is closely similar to that of **8**. Crystals of **8** suitable for X-ray studies could not be obtained, although the species with the oda ligand $[\text{Mn}(\text{oda})(\text{terpy})]$ has been previously reported by us.^[14] The latter cannot be isostructural with **8**, because tda cannot assume the planar *mer* conformation as oda.^[12] Therefore, it is more probable that **8** is structurally similar to **9** (see below) since the tridentate coordination of terpy and pyterpy are rather similar.

Crystals of **9** were obtained from the in situ reaction between an ethanol solution of the pyterpy ligand over a water solution of **1**. Figure 13 shows that **9** is basically a 1D poly-

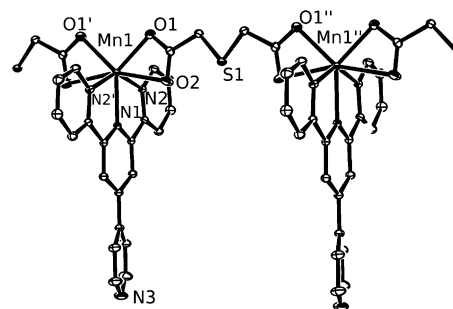


Figure 13. Local coordination of the Mn^{II} ion in the building block of $[\text{Mn}(\text{tda})(\text{pyterpy})]_n$ (**9**). Hydrogen atoms are omitted for clarity. Symmetry transformations used to generate equivalent atoms: $\prime: -x+1, y, -z+1/2$; $\prime\prime: -x+1, y, -z+3/2$.

mer, in which single tda chains extend along the *c* axis (with an uncoordinated sulfur atom). Thus each metal approximately adopts a pentagonal bipyramidal coordination with two carboxylate groups in the equatorial plane together with the N1 atom of the pyterpy central ring. The ligand has twofold symmetry and the N2, N2' donors from two other rings occupy the axial positions. The Mn–O distances are somewhat asymmetric, that is, 2.1826(8) and 2.4861(8) Å, whereas the Mn–N ones are quite similar (Mn–N1 = 2.2197(12) and Mn–N2 = 2.2507(12) Å). Other structural parameters are given in Table 4.

Table 4. Selected bond distances [Å] and angles [°] for **9**.^[a]

Mn1–O1	2.1826(8)	Mn1–N1	2.2197(12)
Mn1–O2	2.4861(8)	Mn1–N2	2.2507(9)
O1–Mn1–O1#1	89.91(4)	O1#1–Mn1–O2	143.22(3)
O1–Mn1–O2	55.86(3)	O1#1–Mn1–O2#1	55.86(3)
O1–Mn1–O2#1	143.22(3)	O1#1–Mn1–N2	110.05(3)
O1–Mn1–N2	95.41(3)	O2–Mn1–O2#1	160.49(4)
O1–Mn1–N2#1	110.05(3)	N1–Mn1–O2#1	80.25(2)
O1–Mn1–N1	135.04(2)	N2–Mn1–O2#1	85.71(3)
N1–Mn1–O2	80.25(2)	N1–Mn1–N2	72.01(2)
N2–Mn1–O2	88.29(3)	N1–Mn1–N2#1	72.01(2)
C2–S1–C2#2	98.58(7)	N2–Mn1–N2#1	144.02(4)

[a] Symmetry transformations used to generate equivalent atoms: #1: $-x+1, y, -z+1/2$; #2: $-x+1, y, -z+3/2$.

The absence of water molecules in the crystal is an indication that π – π stacking is important for the supramolecular arrangement of **9**. As a matter of fact head-to-tail orientations of the adjacent ribbons are featured, as highlighted in Figure S9 in the Supporting Information and Figure 14. The latter shows four parallel ribbons, which are alternatively displaced above and below the plane of the drawing by about 2.5 Å. The two consecutive and fully eclipsing pyterpy ligands at one ribbon are as distant as the cell's *c* axis (10.4 Å). In between them, there is room for two more rings

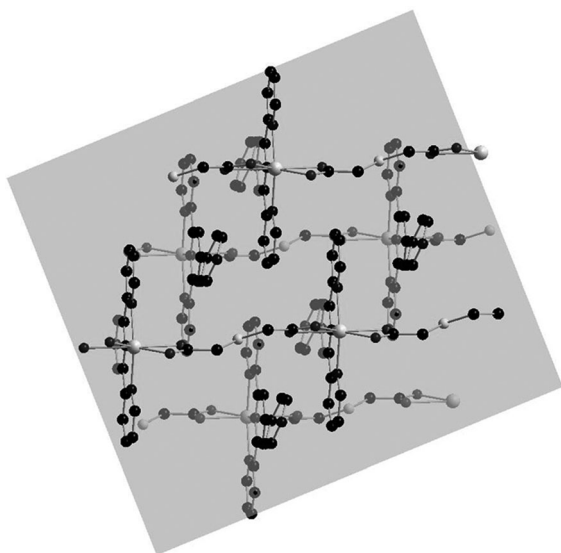


Figure 14. Parallel ribbons in the crystal of $[\text{Mn}(\text{tda})(\text{pyterpy})]_n$ (**9**). As highlighted by the transparent halfway plane, a doubly layered 2D sheet is formed thanks the partial π - π interactions between interpenetrating aromatic N rings in head-to-tail fashion. See colour version of this figure in the Supporting Information.

for the lower and upper ribbons, which are interpenetrated in a head-to-tail fashion. Their eclipsing is only partial and π - π stacking cannot be optimal. In the border region between any two double deck sheets, the N atoms of the pyterpy uncoordinated pyridine rings almost eclipse each other thus introducing a potential repulsion between the lone pairs, which is mitigated by the large separation of 5.2 Å.

The ligand 2,4,6-tris(2-pyridyl)-1,3,5-triazine (tpt) reacts with **1** to produce in situ from the same reaction two different crystalline forms, namely $[\text{Mn}(\text{tda})(\text{tpt})(\text{H}_2\text{O})]\cdot 2\text{H}_2\text{O}$ (**10**) and $[\text{Mn}(\text{tda})(\text{tpt})(\text{H}_2\text{O})]_2\cdot 2\text{H}_2\text{O}$ (**11**). There is evidence (see the Experimental Section) that the former is the kinetic product of the reaction. The structures, presented in Figures 15 and 16 (selected bond distances and angles are given in Table 5) are rather different for their monomeric and dimeric, primary structure, respectively. Similar to **9**, the metal coordination is almost bipyramidal pentagonal. In **10**, tda adopts the typical *fac* coordination with one sulfur and two oxygen atoms (O1 and O3) as donors. The axial ligands are O1 and one H_2O molecule (O5), whereas the sulfur and the O3 atoms occupy with the three tpt N donors the equatorial

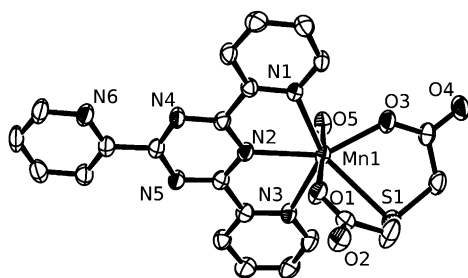


Figure 15. Molecular structure of $[\text{Mn}(\text{tda})(\text{tpt})(\text{H}_2\text{O})]\cdot 2\text{H}_2\text{O}$ (**10**). Hydrogen atoms are omitted for clarity.

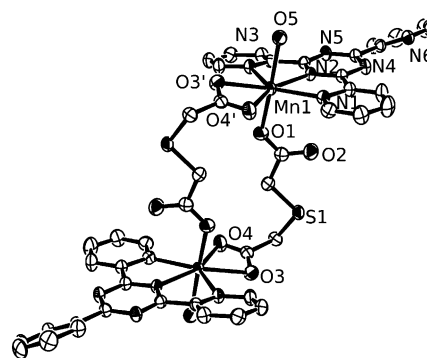


Figure 16. Molecular structure of $[\text{Mn}(\text{tda})(\text{tpt})(\text{H}_2\text{O})]_2\cdot 2\text{H}_2\text{O}$ (**11**). Hydrogen atoms are omitted for clarity. Symmetry transformation used to generate equivalent atoms: $': -x+3/2, -y+1/2, -z+1$.

Table 5. Selected bond distances [Å] and angles [°] for **10** and **11**.

	10		11 ^[a]
Mn1–O1	2.135(2)	Mn1–O1	2.112(2)
Mn1–O3	2.164(3)	Mn1–O3#1	2.286(2)
Mn1–O5	2.175(3)	Mn1–O4#1	2.341(3)
Mn1–N1	2.399(3)	Mn1–O5	2.233(2)
Mn1–N2	2.306(3)	Mn1–N1	2.373(3)
Mn1–N3	2.509(3)	Mn1–N2	2.272(3)
Mn1–S1	2.8406(11)	Mn1–N3	2.412(3)
O1–Mn1–O3	101.02(10)	O1–Mn1–O5	175.69(10)
O1–Mn1–O5	174.29(10)	O1–Mn1–O3#1	92.18(9)
O1–Mn1–N1	85.11(10)	O1–Mn1–O4#1	88.49(10)
O1–Mn1–N2	88.03(10)	O1–Mn1–N1	102.35(10)
O1–Mn1–N3	96.24(10)	O1–Mn1–N2	95.20(9)
O1–Mn1–S1	73.10(7)	O1–Mn1–N3	83.65(10)
O3–Mn1–O5	84.28(10)	O5–Mn1–O3#1	87.31(9)
O3–Mn1–N1	83.30(10)	O5–Mn1–O4#1	94.79(10)
O3–Mn1–N2	149.53(10)	O5–Mn1–N1	80.73(9)
O3–Mn1–N3	138.93(9)	O5–Mn1–N2	83.04(10)
O3–Mn1–S1	71.75(7)	O5–Mn1–N3	92.04(10)
O5–Mn1–N1	97.69(10)	O3#1–Mn1–O4#1	56.65(9)
O5–Mn1–N2	88.28(10)	O3#1–Mn1–N1	138.98(9)
O5–Mn1–N3	78.27(10)	O3#1–Mn1–N2	148.12(9)
O5–Mn1–S1	106.95(8)	O3#1–Mn1–N3	81.73(9)
N1–Mn1–N2	68.41(9)	O4#1–Mn1–N1	85.28(9)
N1–Mn1–N3	135.46(9)	O4#1–Mn1–N2	154.28(9)
N1–Mn1–S1	142.47(7)	O4#1–Mn1–N3	137.31(9)
N2–Mn1–S1	138.42(7)	N1–Mn1–N2	69.05(9)
N2–Mn1–N3	67.15(9)	N1–Mn1–N3	137.39(9)
N3–Mn1–S1	78.24(7)	N2–Mn1–N3	68.39(9)
C3–S1–C2	102.4(2)	C2–S1–C3	99.67(16)

[a] Symmetry transformations used to generate equivalent atoms: #1: $-x+3/2, -y+1/2, -z+1$.

positions of the pentagon (Mn1–S1 = 2.8406(11) and Mn–O3 = 2.164(3) Å). Such a constrained arrangement determines some difference in the Mn–N distances (Mn–N1 = 2.399(3), Mn–N2 = 2.306(3) and Mn–N5 = 2.509(3) Å). In other Mn–tpt complexes,^[38] the bond between Mn from the central tpt N atom is definitely shorter (~2.26 Å^[20]) than the other Mn–N lengths. A hydrogen bonding network in **10** involves solvent water molecules and both the uncoordinated oxygen atoms of tda and the N atom of the uncoordinated tpt pyridine ring (see Figure S10 in the Supporting Informa-

tion). Therefore, the 3D structural arrangement of the monomeric complex unit is possible without any evident ribbon or layered components arising from cooperative π – π stacking.

Complex **11** is a centrosymmetric dimer (Figure 16) also with approximate bipyramidal pentagonal coordination at both the Mn atoms. At variance with the other dimer **7** (Figure 11), the two metals are not in close contact as part of a Mn_2O_2 framework, but are as distant as 8.1 Å due to the pair of stretched tda ligands, which have as in **3–5** an uncoordinated S atom. The carboxylate groups act as monodentate toward one metal (*trans*-axial with respect to one H_2O , O5 donor) and bidentate (with O3 and O4) toward the other. The latter O,O chelate together with the N donor atoms of the tris-chelate tpt ligand forms the equatorial pentagon. The arrangement seems to be more compact than in **10** in which two equatorial donors were the tda's S and O donor atoms, so that the Mn–N distances become more equivalent (Mn1–N1 = 2.373(3), Mn1–N2 = 2.272(3) and Mn1–N5 = 2.412(3) Å).

The tda ligands in **11** hold together only pairs of metals but do not allow the formation of the covalent 1D ribbons as occurs in **3–6**. However, the binuclear building blocks are still extended in ribbons due to the evident hydrogen bonding between the coordinated H_2O molecule and the N6 nitrogen atom of the external tpt pyridine ring (see Figure S11 in the Supporting Information). Moreover, the mentioned ribbons are organized in sheets due to double hydrogen-bonding interactions, which involve, at one side, the H_2O solvent molecule (O6) and the uncoordinated carboxylate oxygen atom (O2) and, at the other side, two already coordinated O atoms (O5 and O3). A layered supramolecular arrangement (plane *ac*) is formed as depicted in Figure 17, which is interestingly compared with that formed in the unique structure of **3**. In both cases, the ribbons are threaded into sheets but the binuclear beads in **11** are covalently connected in one direction and there is not cumulative π – π stacking between the ribbons. The picture is overall dominated by hydrogen bonding. Evidently, the flexibility of the tda coordination mode μ - $\kappa^2(\text{O},\text{O}'),\kappa^1(\text{O}'')$ in **11** (similar to

one organometallic Zr complex^{[39])} determines a very different stereochemical nature with respect to **10** in spite of the same molecular components.

Magnetic studies: Compounds **1** and **3–7** have been magnetically characterized. The molar magnetic susceptibility of compound $[\text{Mn}(\text{tda})(\text{H}_2\text{O})]_n$ (**1**) was measured in the range 1.7–300 K. Both the susceptibility χ_{mol} and its product with temperature ($\chi_{\text{mol}}T$), reported in Figure 18a, show typical paramagnetic behaviour. The $\chi_{\text{mol}}T$ value of $4.38 \text{ cm}^3 \text{ K mol}^{-1}$ at 300 K is indicative of uncorrelated high-spin Mn^{II} ions (theoretical value of 4.38 for five unpaired electrons). On lowering the temperature, $\chi_{\text{mol}}T$ decreases significantly below 150 K, whereas χ_{mol} rises monotonically until it reaches a maximum at 2.1 K. This fact points towards some antiferromagnetic interaction between the manganese ions. A plot of the inverse susceptibility $1/\chi_{\text{mol}}$ versus temperature gives a Curie–Weiss behaviour ($1/\chi_{\text{mol}} = (T - \theta)/C$) with a Curie constant $C = 4.45$ and $\theta = -4.5$ K.

The temperature dependence of the magnetic properties of **3** ($\chi_{\text{mol}}T$ and χ_{mol}) is plotted in Figure 18b. At 300 K, the $\chi_{\text{mol}}T$ product per Mn atom is $3.84 \text{ cm}^3 \text{ K mol}^{-1}$, which is significantly lower than the spin-only value expected for an uncorrelated Mn^{II} ion. On decreasing temperature, $\chi_{\text{mol}}T$ steadily decreases, which indicates that antiferromagnetic interactions are operative in the complex. Indeed χ_{mol} goes through a maximum at 35 K and then declines rapidly, and the curve of $1/\chi_{\text{mol}}$ versus temperature deviates substantially from Curie–Weiss behaviour below 140 K. Fit above that temperature yields $C = 4.48 \text{ cm}^3 \text{ K mol}^{-1}$ and $\theta = -49.1$ K. The Curie constant value is now slightly above the value expected for uncorrelated Mn^{II} ions, and the Curie–Weiss temperature shows a quite strong antiferromagnetic interaction. In view of the centrosymmetric structure, an isotropic antiferromagnetic dimer model [Eq. (1)] was used to fit the experimental $\chi_{\text{mol}}T$ data. The obtained J value of $+8.32 \pm 0.02 \text{ cm}^{-1}$ (with g fixed at 2 as expected for Mn^{II} ions) appears to be rather large for Mn^{II} – Mn^{II} carboxylate dimers.^[40]

$$H = \sum_{i=1,2} \beta g \hat{S}_{\text{Mn}_i} H + J \hat{S}_{\text{Mn}_1} \hat{S}_{\text{Mn}_2} \quad (1)$$

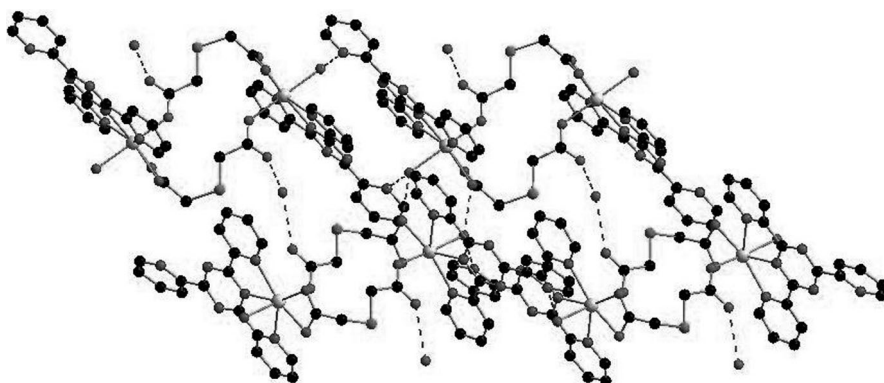


Figure 17. Sheets in the crystal of **11** formed by the horizontal (*a* direction) 1D ribbons with binuclear Mn_2 units. Hydrogen-bonding interactions overall govern the 2D pattern in the *ac* plane. See colour version of this figure in the Supporting Information.

The above model shows some discrepancy of the χ_{mol} data at low temperature (below 30 K). In particular χ_{mol} does not converge to zero as would be expected for full population of the singlet ground state. Impurities (e.g. some oxidized Mn^{III} ion) or partially uncoupled Mn^{II} ions or magnetic anisotropy^[41] can account for this behaviour. Magnetization measurements at low temperature generally help in showing magnetic anisotropy but, in this

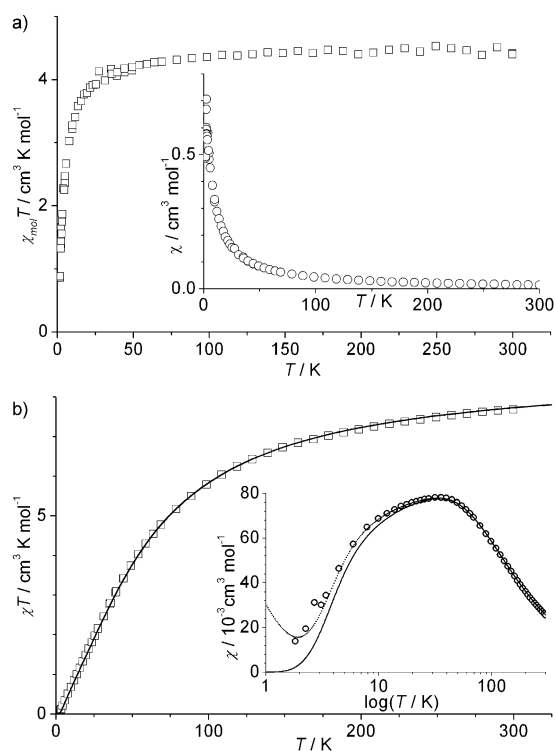


Figure 18. $\chi_{\text{mol}}T$ versus T plots for compounds **1** and **3** (a and b, respectively). The insets show the corresponding χ_{mol} versus T (for **1**) or $\log(T/K)$ (for **3**) plots (—: fully isotropic model;: anisotropic model, as deduced from HF-EPR; see text for parameters).

case, the singlet ground state prevents such an approach. We resorted then to high-field electron paramagnetic resonance to clarify the matter (see below).

Due to the structural similarity of the cores, the magnetic behaviours of **4** and **5** are comparable and the discussion will be limited to **4**. The observed $\chi_{\text{mol}}T$ value at room temperature per Mn ion ($4.06 \text{ cm}^3 \text{ K mol}^{-1}$) is again significantly lower than that expected for non-interacting centres. The subsequent decrease of $\chi_{\text{mol}}T$ on lowering temperature (Figure 19) strongly suggests antiferromagnetic coupling, an hypothesis that is confirmed by a well-defined maximum in the χ_{mol} versus T curve at 22 K. Magnetic data were again fitted with Equation (1) by assuming identical Landé factors for both Mn^{II} : $g = 2.008 \pm 0.003$, $J = +5.54 \pm 0.02$ and an agreement factor $R^2 = 0.99998$ ($R^2 = 0.99947$ for fit of the χ_{mol} curve that yielded the same best-fit values). The value of J is such that a field-induced spin ground state transition from $S = 0$ to $S = 1$ may occur at around 6 T. Such a transition is partially observed in the M versus H curve measured at 2.5 K and it is nicely simulated for $J = +5.5 \pm 0.1 \text{ cm}^{-1}$ (see Figure S12 in the Supporting Information). Therefore, **3** and **4** exhibit very similar exchange coupling that is certainly due to the presence of acetate bridging modes in both cases. Nevertheless, whereas in the former case the unusual trigonal prismatic geometry accompanies to a pronounced magnetic anisotropy, which is unusual for Mn^{II} , in the latter case

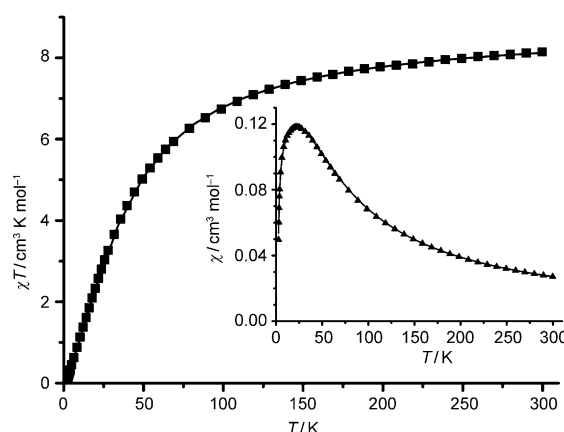


Figure 19. $\chi_{\text{mol}}T$ versus T plot for compound **4** with best-fit curve. The inset shows the corresponding χ versus T plot with its best-fit curve.

the local octahedral geometry is reflected by a featureless isotropic magnetic behaviour.

Also for the polymeric complex **6**, the variations of the susceptibility χ_{mol} and of its product with the temperature $\chi_{\text{mol}}T$ were monitored (see Figure S13 in the Supporting Information). The results are similar to that of **1**. At 300 K, the value of $\chi_{\text{mol}}T$ is $4.33 \text{ cm}^3 \text{ K mol}^{-1}$ (in agreement with uncorrelated high-spin Mn^{II} ions) and the product starts to decrease significantly below 150 K. The susceptibility χ_{mol} reaches a maximum value at 2.6 K in agreement with a weak antiferromagnetic interaction between metal ions. Indeed fitting $1/\chi_{\text{mol}}$ versus temperature with a Curie–Weiss law gives $C = 4.39 \text{ cm}^3 \text{ K mol}^{-1}$, yielding $g = 2.00$, and a θ of only -3.8 K .

The temperature dependence of the magnetic properties of **7** ($\chi_{\text{mol}}T$ and χ_{mol}) is plotted in Figure 20. At 300 K, the $\chi_{\text{mol}}T$ product atom is $8.52 \text{ cm}^3 \text{ K mol}^{-1}$, slightly lower than the spin-only value expected for two uncorrelated Mn^{II} ions ($8.75 \text{ cm}^3 \text{ K mol}^{-1}$). On decreasing the temperature, $\chi_{\text{mol}}T$ does not significantly vary down to 100 K, then it starts increasing steadily up to the maximum of $12.4 \text{ cm}^3 \text{ K mol}^{-1}$, which indicates that a weak ferromagnetic interaction is operative in the binuclear unit. The magnitude of χ_{mol} is seen to follow a Curie–Weiss law, as the fit of $1/\chi_{\text{mol}}$ versus temperature gives the values $C = 8.51 \text{ cm}^3 \text{ K mol}^{-1}$ and $\theta = +1.71 \text{ K}$.

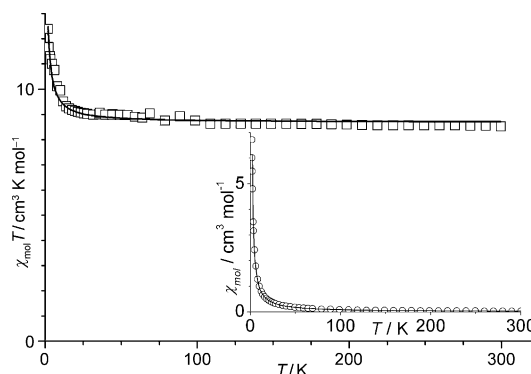


Figure 20. $\chi_{\text{mol}}T$ versus T plot for compound **7** with best-fit curve. The inset shows the corresponding χ_{mol} versus T plot.

The experimental data were satisfactorily fit by using Equation (1) and assuming identical Landé factors for both the Mn^{II} ions ($g = 1.991 \pm 0.004$, $J = -0.24 \pm 0.01 \text{ cm}^{-1}$, agreement factor $R^2 = 0.95066$). The small ferromagnetic interaction reflects the difference in the bridging mode for compound **7** with respect to compounds **3–5**, but it is quite unusual for $\text{Mn}_2(\mu^2\text{-O})_2$ cores in which the typical magnetic interactions are strongly antiferromagnetic. Magnetization curves at low temperature (not shown) showed no nesting effect, which is symptomatic of magnetic anisotropy, as expected for isotropic Mn^{II} .

High-field high-frequency electron paramagnetic resonance study of complex $[\text{Mn}(\text{tda})(\text{bipy})]_n$ (3**):** In view of the unusual coordination sphere of **3** and its magnetic anisotropy, high-field high-frequency EPR (HF-EPR) studies were performed. Especially, in the strong field limit, spectra are largely simplified due to the zero-field splitting (ZFS) terms becoming only a perturbative effect on the leading Zeeman effect. Transitions along the principal axes are then observed as series of regularly spaced signals, allowing direct reading of the $|D|$ and $|E|$ values out of the spectrum. The sign of D can generally also be determined from low-temperature measurements, monitoring depopulation effects within a spin manifold. In the literature, there are not many thorough studies of dimers with S -type ions, but mainly of high-spin $d^5 \text{Fe}^{\text{III}}$ and Mn^{II} compounds.^[42]

The spectra, measured on pellets at variable temperature at 190 and 285 GHz, are reported in Figure 21. At both 190 and 285 GHz, the transitions can be divided into two main

groups. The first extends roughly over 3 T around the $g=2$ position (6.8 T and 10.2 T for 190 and 285 GHz respectively), with the signals varying with a $g=2$ dependence. At 285 GHz, these signals appear between 8.7 and 11.7 T. The second group is observed at low fields (below 5 or 8 T at 190 and 285 GHz respectively), with signals corresponding to so-called forbidden transitions with a typical $g \gg 2$ dependence on changing the frequency. At 190 GHz, also a third group of signals appears at fields higher than 8.5 T. These are actually signals due to the contamination of this frequency by a small 285 GHz component and can then be overlooked. The first group of transitions is most important for our analysis.

At 3 K, three well-defined features appear at 5.4, 6.7 and 8.3 T at 190 GHz and at 8.5, 10.2 and 11.7 T at 285 GHz. At this temperature, only the lowest M_S levels are expected to be thermally populated, which implies that the system has three principal axes associated to a large rhombicity. An increase of the temperature to 5 K lowers the intensity of the signals, confirming that they originate from the ground spin level. As a result, these signals cannot be assigned to a dimeric Mn_2 unit, with $S=0$ ground state up to ~ 8 T (see discussion and Figure S15 in the Supporting Information). Rather, the signals are assigned to a monomeric Mn^{II} entity, the presence of which could already be inferred from the susceptibility measurement.^[43]

Even if the monomer is present at low concentrations, the increased sensitivity at low temperatures allows its EPR signature to be observed. At higher temperatures, the pattern of a rhombic $S=5/2$ is confirmed with the observation of signals at 6.06(9.48) and 7.55(10.96) T at 190(285) GHz. The $S=5/2$ structure is nicely reproduced with the following parameters: $D = 0.35 \text{ cm}^{-1}$, $E = 0.107 \text{ cm}^{-1}$ and $g = 2.0$. However, a single $S=5/2$ system cannot account for all the signals, which appear at increasing temperatures, and the additional resonances are attributable to the excited spin states of the Mn dimer. With the reasonable assumption that the monomeric entity is closely related to the dimeric unit, we exploited the ZFS parameters previously obtained as starting values of the single-ion contribution to the global ZFS of the successive spin states of the dimer.^[44] For the $S=1$ state, the projection coefficient is $-2 \cdot 16/5 = -6.4$; thus the single-ion contribution for D is expected to be of the order of -2 cm^{-1} with an important rhombicity. For the next spin levels ($S=2, \dots$), the projection coefficients are progressively smaller and should result in single-ion ZFS of the order of -0.3 cm^{-1} for $S=2$ and smaller for the other ones. Besides the single-ion term, the dipolar interaction also contributes to the magnetic anisotropy. This can be estimated to be $|D_{\text{dip}}| \approx 0.12 \text{ cm}^{-1}$ by using the point dipole approximation [Eq. (2)]^[44] with $r = 3.502 \text{ \AA}$ and $g = 2$.

$$D_{\text{dip}} = \frac{3\mu_B^2 g^2}{r^3} \quad (2)$$

For the $S=1$ state, the value is amplified by the projection coefficient of $+3.7$, and the D term is about 0.4 cm^{-1} . For

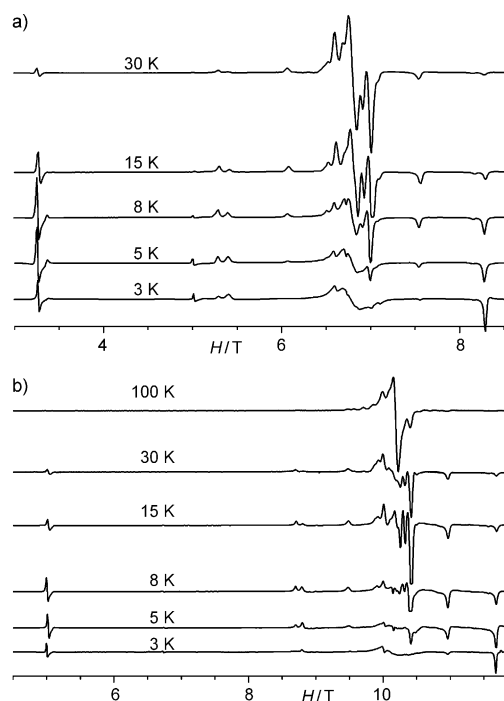


Figure 21. Variable-temperature HF-EPR spectra for compound **3** a) at 190 GHz and b) at 285 GHz (traces at 3 and 30 K were scaled arbitrarily by $\times 2$ and $\times 5$, respectively, see the Experimental Section).

the next spin levels, the projection coefficients are even smaller. Unfortunately, the analysis cannot be further developed in the absence of information on the principal axes of the single-ion term. The total ZFS of the spin states of the dimer is roughly estimated in the range from -1.6 to -2.4 cm^{-1} for the $S=1$ state, from -0.3 to -0.5 cm^{-1} for the $S=2$ state, and smaller for the higher spin states. In the spectra, extra signals at about 1.4 T from the $g=2$ position are observed at 5.3(8.7) and 8.2(11.6) T at 190(285) GHz. These signals exhibit the temperature dependence expected for the $S=1$ transitions, with larger intensity when the temperature increases from 3 to 5 K. The resonance positions of these signals are satisfactorily reproduced with $D = -1.4\text{ cm}^{-1}$, $E = 0.4\text{ cm}^{-1}$ and $g = 2.0$. In view of the many hypotheses and simplifications, these results nicely agree with the above estimates. No value for the higher spin levels of the dimer was derived, because the signals from these levels are expected to fall mostly in the $g=2$ region, which is vastly crowded. However the observation of so many lines in this region is also in favour of the above analysis.

We calculated the corresponding triplet and the spectra of isolated Mn^{II} ions by using the mentioned parameters (see Figure 22 and Figures S16 and S17 in the Supporting Information). Scaling of both contributions can only be approximative, since the percentage of the triplet state is varying with both temperature and magnetic field (see Figure S15 in the Supporting Information). However a fair agreement is found for the limiting 1/10 amount of Mn^{II} (see Figure S16 in the Supporting Information). Though no information is available on the tensor alignment, we used the set of J , g , D_i and E_i parameters to simulate the χ_{mol} curve through full diagonalization of the Hamiltonian. To do so we simplified by considering all tensors parallel. We also considered anisotropic exchange as given by D_{dip} . Agreement is excellent considering some 1.2% uncoupled Mn^{II} (see the dotted curve in Figure 18b), the difference with HF-EPR being accountable by the roughness of the hypotheses.

Conclusion

The thiodiacetate ligand with up to five potential donor atoms shows a variety of behaviours toward transition-metal ions.^[12,15,24] Mn^{II} is peculiar for containing one unpaired electron in each d orbital, hence it has no particular bias toward a preferential coordination mode. Therefore, the possibilities of wrapping tda around one or more metal centres are numerous and the eleven compounds reported in this paper show a variety of features in spite of the similar components and synthetic procedures. In particular, we have attempted to draw correlations between the different supramolecular arrangements, which are governed by π - π bonding interactions or hydrogen bonding or a mixture of them. Our study show that the self-assembling capabilities of aromatic nitrogen co-ligands can even be more determinant than the hydrogen bonding, which is stronger by a factor of three or four times.^[45] In particular, when the small dispersion forces

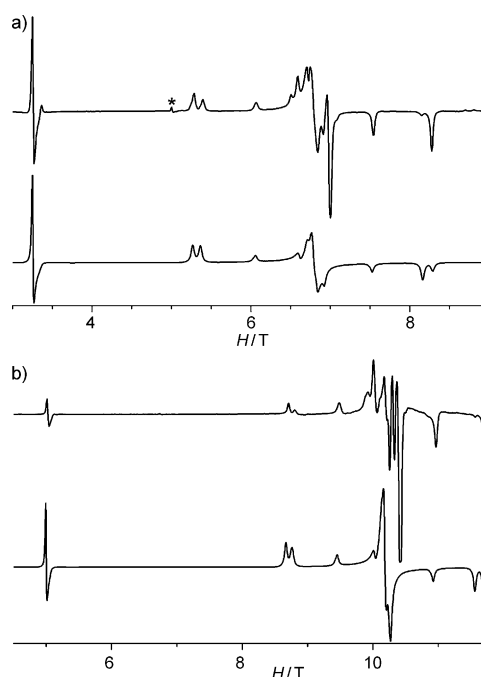


Figure 22. Experimental (up) and simulated (down) spectra for compound **3** a) at 8 K and 190 GHz (the * resonance corresponds to the $S=1$ forbidden transition at 285 GHz, see text) and b) at 15 K and 285 GHz. See Figures S16 and S17 in the Supporting Information for the other temperatures and details of the scaling process.

(van der Waals) of the π - π stacking accumulate together in an extended and compact bifacial arrangement, the system can even expel all water molecules and even adopt a less favourable coordination mode at the metal. Thus, in $[\text{Mn}(\text{tda}(\text{bipy}))_n]$ (**3**) the trigonal prism is preferred to the octahedron with an evident overturn of one paradigm of supramolecular chemistry, that is, the selection of a rigid metal building block to obtain desired spatial properties. The latter remains generally true, since the different Mn^{II} coordination mode in **3** has a little energy cost, such as that corresponding to a different, yet extended, supramolecular pattern. This was already pointed out^[15b] in view of the fact that even the smallest bipy substituents prevent the optimal π - π stacking and allow entrance of water molecules in the coordination sphere with their added hydrogen-bonding energy (compound **4-6**). Indirect computational validation of these trends, based on bimetallic molecular models, has been obtained with the DFT approach. The unicity of **3** has been also highlighted by the magnetic and EPR measurements that indicate a pronounced anisotropy, hence a major difference with respect to the typical Mn^{II} octahedral compounds, which have isotropic magnetic behaviour. Besides the indicated important results, the paper correlates in detail the variety of structural cases in which the competition between hydrogen bonding and π - π stacking is determinant for formation of 1D ribbons (through covalent or hydrogen-bonding interactions), as well as their threading into 2D layers or in actual 3D arrangements.

Experimental Section

General procedures: All preparations and other operations were carried out under aerobic conditions. Thiodiacetic acid and other chemicals were obtained from commercial sources and were used without further purification. Microanalyses (C, H, N) were carried out by the Microanalytical Services of CITIUS (University of Sevilla). IR spectra were recorded on Perkin–Elmer Model 883 spectrophotometer (Nujol emulsion in NaCl plates). Syntheses of complexes **4** and **5** were previously reported.^[15b]

[Mn(tda)(H₂O)]_n (1**):** Na₂CO₃ (0.21 g, 2 mmol) was added to a solution of S(CH₂COOH)₂ (0.30 g, 2 mmol) in water (20 mL). The mixture was stirred until the evolution of CO₂ ceased and then added onto a solution of MnCl₂·4H₂O (0.30 g, 2 mmol) in water (15 mL). The resulting mixture was stirred for 10 min. Then, acetone was added and the solution was kept at room temperature overnight. Colourless crystals of **1** were formed, filtered off, washed with water, acetone and Et₂O and air-dried (0.30 g, 68%). IR (NaCl): $\tilde{\nu}$ = 3530–3051 (br, OH), 1591 cm^{−1} (s, COO asym.); μ = 5.6, μ_B at 23 °C; elemental analysis: calcd (%) for C₄H₆MnO₅S (221.09): C 21.72, H 2.71; found: C 21.44, H 2.91.

Deuterated compound [Mn(tda)(D₂O)]_n was obtained as a microcrystalline solid in 63% yield (0.28 g for a 2 mmol scale) by following the same experimental procedure, but by using deuterated water as the reaction medium and working under a N₂ atmosphere. IR (NaCl): $\tilde{\nu}$ = 2460 (s), 2351 (s, OD), 1637 (vs) 1590 cm^{−1} (vs, COO asym.).

[Mn(tda)(H₂O)₃·H₂O (2**):** The compound was prepared by following the same procedure reported for **1**. The difference was the crystallization of the final resulting aqueous solution that was kept exposed to air at room temperature without the addition of acetone. Slow evaporation of water resulted in two types of crystals: block-shaped colourless **2** (0.25 g, by starting from 2 mmol of MnCl₂·4H₂O, 46%) and needle-shaped microcrystals of **1** (0.10 g, 23%). Both were filtered off, washed with water, acetone and Et₂O, air-dried and separated manually. IR (NaCl): $\tilde{\nu}$ = 3499 (m), 3430 (s), 3400–3030 (br), 1642 (s), 1566 (s), 1414 (s), 1381 (m), 1261 (m), 1247 (s), 1178 (m), 947 (m), 927 (m), 880 (w), 794 (s), 768 (s), 721 (s), 682 cm^{−1} (s); elemental analysis: calcd (%) for C₄H₁₂O₈SMn (275.14): C 17.46, H 4.40, S 11.65; found: C 17.56, H 4.01, S 11.76.

[Mn(tda)(bipy)]_n (3**):** Bipy (0.08 g, 0.5 mmol) was added to a solution containing **1** (0.11 g, 0.5 mmol) in hot water (15 mL). The resulting mixture was stirred at reflux until a clear yellow solution was obtained. Compound **3** crystallized upon evaporation of the solvent at room temperature after a few days. Yellow crystals were filtered off, washed with cold water and Et₂O and dried in air (0.15 g, 84%). Recrystallization of the product in water results in the formation of yellow crystals suitable for an X-ray study. IR (NaCl): $\tilde{\nu}$ = 3098, 3062 (w, CH, bipy), 1594 cm^{−1} (s, COO asym.); elemental analysis: calcd (%) for C₁₄H₁₂MnN₂O₄S (359.26): C 46.76, H 3.34, N 7.79; found: C 46.74, H 3.33, N 8.01.

[Mn(tda)(4,4'-(MeO)₂bipy)]₂·2H₂O (6**):** A solution of compound [Mn(tda)(H₂O)]_n (0.113 g, 0.5 mmol) in water (20 mL) was treated with a solution of 4,4'-dimethoxy-2,2'-bipyridine ((MeO)₂bipy, 0.123 g, 0.5 mmol) in ethanol (20 mL). The mixture was heated at 90 °C for 2 h and then it was concentrated to a volume of 15 mL. The solution was filtered and yellow crystals of **6**, suitable for single-crystal X-ray structure analysis, were obtained after slow evaporation of the solvent at ambient temperature for several days. Yield: 0.18 g (79% yield); IR (NaCl): $\tilde{\nu}$ = 3653–3065 (br), 1643 (s), 1606 (vs), 1567 (vs), 1538 (s), 1504 (s), 1495 (s), 1467 (vs), 1453 (vs), 1410 (s), 1398 (s), 1367 (vs), 1339 (s), 1280 (s), 1243 (s), 1225 (s), 1164 (w), 1088 (w), 1033 (s), 1020 (s), 1002 (s), 970 (w), 935 (m), 924 (m), 876 (w), 862 (m), 840 (s), 824 (s), 794 (m), 766 (m), 735 (w), 682 (s), 664 cm^{−1} (w); elemental analysis: calcd (%) for C₁₆H₂₀N₂O₈SMn (455.34): calcd C 42.20, H 4.43, N 6.15; found: C 42.25, H 4.26, N 6.08.

[Mn(tda)(phen)]₂·6H₂O (7**):** Compound **7** was prepared in a similar manner to that described for **3**, by using **1** (0.11 g, 0.5 mmol) and *o*-phen-H₂O (0.10 g, 0.5 mmol). Yellow crystals were filtered off, washed with cold water and Et₂O and air-dried (0.17 g, 83%). IR (NaCl): $\tilde{\nu}$ = 3664–3097 (br), 3063 (w), 1645 (vs), 1588 (vs), 1519 (s), 1491 (w), 1461 (m), 1426 (s), 1373 (s), 1346 (w), 1316 (s), 1244 (w), 1221 (s), 1182 (w), 1140 (s), 1099 (m), 937 (m), 921 (m), 865 (s), 854 (s), 780 (w), 768 (w),

727 (s), 715 (s), 683 (w), 662 (w), 642 cm^{−1} (w); μ = 5.2, μ_B at 23.5 °C; elemental analysis: calcd (%) for C₁₆H₁₈N₂O₇SMn (437.33): C 43.94, H 4.15, N 6.41; found: C 45.07, H 3.97, N 6.67.

Compound [Mn(tda)(phen)]₂ was obtained by heating compound **7** at 45 °C for several hours. Elemental analysis: calcd (%) for C₁₆H₁₂N₂O₄SMn (383.28): C 50.14, H 3.16, N 7.31, S 8.37; found: C 49.22, H 3.17, N 7.34, S 8.34.

[Mn(tda)(terpy)]_n (8**):** Terpyridine (0.12 g, 0.5 mmol) was added to a solution of **1** (0.11 g, 0.5 mmol) in water (30 mL). Immediately, a microcrystalline yellow precipitate was formed. After 10 min of stirring, the suspension was filtered off and the solid was collected by filtration, washed with water, acetone and Et₂O and air-dried (0.18 g, 80%). IR (NaCl): $\tilde{\nu}$ = 3097 (w), 3067 (w), 1594 (vs), 1577 (vs), 1448 (vs), 1386 (s), 1310 (m), 1297 (w), 1253 (m), 1233 (w), 1188 (s), 1148 (m), 1053 (w), 1013 (w), 986 (w), 920 (s), 877 (w), 824 (w), 789 (m), 769 (s), 740 (w), 666 (m), 651 (m), 636 cm^{−1} (w); μ = 5.9, μ_B at 24 °C; elemental analysis: calcd (%) for C₁₉H₁₅N₃O₄SMn (436.34): C 52.30, H 3.46, N 9.63; found: C 52.08, H 3.61, N 9.93.

[Mn(tda)(pyterpy)]_n (9**):** A 1:1 mixture of water and ethanol (20 mL) was added to a mixture of **1** (0.113 g, 0.5 mmol) and pyterpy (0.155 g, 0.5 mmol). The resulting suspension was stirred for 2 h with heating until the solid was dissolved. From the resulting solution, a yellow precipitate was formed after stirring overnight. The solid was collected by filtration, washed with water, acetone and diethyl ether and air-dried (0.24 g, 93%). IR (NaCl): $\tilde{\nu}$ = 3095 (w), 3065 (w), 1611 (w), 1595 (vs), 1581 (vs), 1564 (s), 1556 (vs), 1542 (s), 1462 (s), 1397 (s), 1341 (w), 1300 (m), 1268 (w), 1245 (s), 1202 (s), 1157 (m), 1088 (m), 1055 (m), 1012 (s), 994 (m), 967 (m), 922 (s), 904 (s), 896 (m), 826 (s), 787 (ms), 747 (s), 728 (s), 683 (m), 669 (w), 655 (s), 634 (s), 620 cm^{−1} (s); elemental analysis: calcd (%) for C₂₃H₁₈N₄O₄SMn (513.43): C 56.14, H 3.53, N 10.91; found: C 56.36, H 3.39, N 10.93.

[Mn(tda)(tpt)(H₂O)]₂·2H₂O (10**) and [Mn(tda)(tpt)(H₂O)]₂·2H₂O (**11**):** Ethanol (7 mL) was slowly added over a solution of **1** (0.11 g, 0.5 mmol) in water (15 mL). Then, a solution of tpt (0.157 g, 0.5 mmol) in ethanol (15 mL) was slowly added over the previous mixture. The test tube was closed and kept in repose for 4 weeks. Two different compounds were obtained as orange and yellow crystals, which were collected by filtration, washed with water, acetone and Et₂O, air-dried and separated manually.

[Mn(tda)(tpt)(H₂O)]₂·2H₂O (10**):** Yellow crystals (0.04 g, 14%); IR (NaCl): $\tilde{\nu}$ = 3680–3001 (br), 1651 (s), 1583 (vs), 1550 (vs), 1526 (vs), 1488 (s), 1469 (s), 1440 (s), 1403 (s), 1381 (s), 1300 (m), 1256 (s), 1243 (s), 1199 (w), 1183 (w), 1164 (m), 1115 (w), 1093 (m), 1080 (w), 1056 (m), 1047 (m), 1039 (m), 1006 (s), 975 (w), 938 (s), 916 (s), 885 (w), 863 (s), 859 (s), 824 (s), 802 (s), 778 (s), 756 (s), 738 (m), 674 (s), 666 (s), 628 cm^{−1} (s); μ = 5.8, μ_B at 29 °C; elemental analysis: calcd (%) for C₂₂H₂₂N₆O₇SMn (569.45): C 46.40, H 3.89, N 14.76; found: C 46.44, H 3.69, N 15.19. Yellow crystals of compound **10** were obtained as the major product in ca. 80% yield, when the diffusion of the ethanol solution of tpt reagent was performed more rapid and directly over the aqueous solution of **1**.

[Mn(tda)(tpt)(H₂O)]₂·2H₂O (11**):** Orange crystals (0.22 g, 80%); IR (NaCl): $\tilde{\nu}$ = 3634–3010 (br), 1670 (m), 1606 (vs), 1571 (vs), 1545 (vs), 1530 (vs), 1467 (s), 1452 (s), 1422 (s), 1407 (s), 1377 (s), 1297 (m), 1290 (m), 1262 (s), 1252 (s), 1234 (s), 1157 (s), 1145 (s), 1135 (s), 1103 (w), 1077 (w), 1046 (m), 1040 (m), 1008 (s), 934 (m), 926 (m), 913 (w), 902 (w), 859 (s), 850 (m), 777 (s), 759 (s), 722 (s), 677 (s), 667 (s), 632 (s), 626 (s), 613 cm^{−1} (s); elemental analysis: calcd (%) for C₂₂H₂₀N₆O₆SMn (551.43): C 47.92, H 3.66, N 15.24; found: C 47.88, H 3.33, N 14.93.

Computational details: The geometries of calculated complexes [Mn₂(μ-OOCH)₄(bipy)₂], **3a** and **3b** and [Mn₂(bipy)₂(OOCH)₂(μ-OOCH)₂(μ-H₂O)] **4a** were computed within the density functional theory at the unrestricted BP86^[46] level of theory by using the 6-31G* basis set. The multiplicity was imposed to S = 5, in agreement with the experimental data recorded at room temperature. Vibrational frequency calculations by diagonalization of the analytically computed Hessian were computed for all models. Structures **3b** and **4a** (both optimized without symmetry constraints) correspond to real minimums in the potential energy surface. Conversely, **3a** (imposed D_{2h} symmetry) is characterized by six imaginary frequencies that involve displacement of some atoms to break the im-

posed symmetry (all of them smaller than 60 cm^{-1}). For the energy differences, single-point calculations on the previously optimized structures were carried out with the 6-311+G** basis set. Coordinates of the optimized compounds are available upon request. All the calculations were performed with the Gaussian 98 package of programs.^[47]

Magnetic measurements: Magnetic moments at room temperature were measured in the solid state with a Sherwood Scientific (Cambridge Research Laboratory) magnetic balance. Magnetic susceptibility and magnetization measurements on pellets made from powdered samples were performed on a Cryogenics S600 SQUID magnetometer operating between 0 and 6 T in the range 2–300 K. Molar susceptibilities were corrected by using Pascal's constants.^[48] Magnetic simulations were performed with a modified version of the Magpack software.^[49] In those procedures the exchange interaction Hamiltonian is defined as $\hat{H} = -2S_1S_2$, so care had to be taken in converting values of J and D_{12} .

HF-EPR measurements: HF-EPR spectra of compound **3** were recorded at the Grenoble High Magnetic Field Laboratory on a previously described homemade spectrometer by using Gunn diodes as source excitation and higher harmonic multipliers.^[50] Powder (190 GHz spectra and 3 and 30 K 285 GHz spectra) or crushed single crystals (remaining 285 GHz spectra) were pressed in pellets to avoid orientation effects. Spectra were analyzed and simulated through full diagonalization of the spin Hamiltonian matrix by using the SIM program^[51] developed by Prof. H. Weihe, Department of Chemistry, University of Copenhagen (calculations used lorentzian shapes with identical 250 G bandwidth).

Powder diffraction data collection and structure determination: X-ray powder diffraction pattern (XRPD) used for the structure determination and Rietveld refinement of **1** was collected according to the step scanning procedure on a Philips X'PERT PRO diffractometer. The $\text{Cu}_{K\alpha}$ radiation was used together with a PIXcel solid-state fast detector in the 2θ range $10\text{--}115^\circ$. Indexing was performed by using an enhanced version of the TREOR program.^[52] The structure of **1** was solved by using the EXPO2009 program.^[53] The software optimizes a molecular structural model based on building blocks defined with internal coordinates. Optimization was performed by comparing the XRPD patterns calculated from randomly generated configurations and using the "integrated Rwp" (iRwp) as the cost function. The starting model of $[\text{Mn}(\text{tda})\text{H}_2\text{O}]$ group was based on the refined structure of **2**, after removing the water molecules, which lie *trans* to the carboxylate groups. The Rietveld refinement of **1** was performed by using the GSAS program.^[54] The comparisons of the calculated and observed powder diffraction patterns are given in Figure S18 (Supporting Information). Crystallographic data and refinement details are reported in Table 6. The zero shift, the cell parameters, the background and profile shape parameters were all refined. A corrected

Table 6. Structural data and refinement details for $[\text{Mn}(\text{tda})(\text{H}_2\text{O})]_n$ (**1**).

Empirical formula	$\text{C}_4\text{H}_6\text{MnO}_5\text{S}$
Molecular mass	221.09
λ [Å]	1.54056
Crystal system	monoclinic
Space group	$P2_1$
a [Å]	7.89760(8)
b [Å]	5.26566(6)
c [Å]	9.06280(8)
α [°]	90
β [°]	116.5881(6)
γ [°]	90
V [Å ³]	337.029(6)
Z	2
D_{calcd} [Mg m ⁻³]	2.106
no. of data	15003
no. of reflections	793
no. of parameters	86
no. of restraints	0
R_p [a]	0.014
R_{wp} [b]	0.018
R_{p2} [c]	0.098
GOF [d]	1.22

[a] $R_p = \sum |I_o - I_c| / \sum I_o$. [b] $R_{wp} = [\sum w(I_o - I_c)^2 / \sum w I_o^2]^{1/2}$. [c] $R_{p2} = \sum |F_o^2 - F_c^2| / \sum |F_o^2|$. [d] $GOF = [\sum w(I_o - I_c)^2 / (N_o - N_{var})]^{1/2}$.

pseudo Voigt profile function with two terms for the correction of asymmetry at the low-angle region was used. The atomic coordinates were first refined by restraining the interatomic distances but, in the final cycles, without any restrain. The isotropic thermal parameters were refined by constraining the shifts of the light atoms all at a unique value, whereas the U_{iso} values of the Mn and S atoms were independently refined. At the end of the refinement, the shifts in all parameters were less than their standard deviations.

Single-crystal data collection and structure determination: A summary of the crystallographic data and structure refinement results for compounds **2**, **6–7** and **9–11** is given in Table 7. Crystallographic data for compounds **3–5** were previously reported.^[15] The X-ray data were collected on three different equipments: An Enraf–Nonius CAD4 diffractometer equipped with a graphite monochromator and $\text{Mo}_{K\alpha}$ radiation (for **6–7** and **11**), Phillips PW1100 FEBO diffractometer equipped with a graphite monochromator and $\text{Cu}_{K\alpha}$ radiation (for **10**) and Bruker–Nonius X8APEX-II

Table 7. Crystallographic data for compounds **2**, **6–7** and **9–11**.

	2	6	7	9	10	11
Empirical formula	$\text{C}_4\text{H}_{12}\text{MnO}_8\text{S}$	$\text{C}_{16}\text{H}_{20}\text{MnN}_2\text{O}_8\text{S}$	$\text{C}_{32}\text{H}_{36}\text{Mn}_2\text{N}_4\text{O}_{14}\text{S}_2$	$\text{C}_{24}\text{H}_{18}\text{MnN}_4\text{O}_4\text{S}$	$\text{C}_{22}\text{H}_{22}\text{MnN}_6\text{O}_7\text{S}$	$\text{C}_{44}\text{H}_{40}\text{Mn}_2\text{N}_{12}\text{O}_{12}\text{S}_2$
Molecular mass	275.14	455.34	874.65	513.42	569.46	1102.88
Crystal system	orthorhombic	monoclinic	monoclinic	monoclinic	monoclinic	monoclinic
Space group	$P2_12_12_1$	$P2_1/n$	$C2/c$	$C2/c$	$P2_1/c$	$C2/c$
a [Å]	7.7074(2)	12.071(3)	21.066(10)	8.7137(2)	15.083(4)	15.491(4)
b [Å]	9.3774(3)	9.446(2)	13.243(7)	24.5784(4)	10.4950(10)	16.995(3)
c [Å]	14.2584(4)	17.283(2)	13.705(6)	10.3873(2)	15.467(4)	17.163(3)
α [°]	90	90	90	90	90	90
β [°]	90	105.53(1)	110.03(4)	107.938(1)	106.58(2)	96.074(18)
γ [°]	90	90	90	90	90	90
V [Å ³]	1030.53(5)	1898.7(7)	3592(3)	2116.50(7)	2346.1(8)	4493.1(16)
Z	4	4	8	4	4	4
D_{calcd} [Mg m ⁻³]	1.773	1.593	1.617	1.611	1.612	1.630
μ [mm ⁻¹]	1.500	0.853	0.894	0.765	0.71	0.735
T [K]	100(2)	293(2)	293(2)	100(2)	293(2)	293(2)
$F(000)$	564	940	1800	1052	1172	2264
independent reflections	3111	3337	3167	3243	4125	3944
R [$I > 2\sigma(I)$]	0.0136	0.0432	0.051	0.0243	0.042	0.045
wR_2 (all data)	0.0370	0.1128	0.154	0.0750	0.149	0.123

CCD diffractometer equipped with a graphite monochromator and $\text{Mo}_{\text{K}\alpha}$ radiation (for **2** and **9**). Unit-cell parameters for compounds **6–7** and **10** and **11** were determined by least-squares refinement of the setting angles of 25 carefully centred reflections. The intensities I were assigned a standard deviation $\sigma(I)$ calculated by using a value of 0.03 for the instability factor k .^[55] They were corrected for Lorentz-polarization effects and an absorption correction was applied.^[56] Atomic scattering factors for neutral atoms were taken from ref. [57]. Both $\Delta f'$ and $\Delta f''$ components of anomalous dispersion were included for all non-hydrogen atoms.^[58] The structures were solved by direct methods (SIR97)^[59] and refined by full-matrix F^2 refinement (SHELX97),^[60] with anisotropic thermal parameters assigned to all non-hydrogen atoms. The hydrogen atoms were introduced in calculated positions. The calculations were performed on a Pentium processor, by using the package WINGX^[61] (ORTEP-III^[62]). Single crystals of suitable sizes of compounds **2** and **9** coated with dry perfluoropolyether were mounted on a glass fiber and fixed in a cold nitrogen stream [$T=173(2)$ K] to the goniometer head. Data collection was performed by means of ω and ϕ scans. The data were reduced (SAINT)^[63] and corrected for Lorentz polarisation effects and absorption by multi-scan method applied by SADABS.^[64] The structure was solved by direct methods (SIR-2002)^[65] and refined against all F^2 data by full-matrix least-squares techniques (SHELXTL-6.12).^[66] All the non-hydrogen atoms were refined with anisotropic displacement parameters. The hydrogen atoms were included from calculated positions and refined riding on their respective carbon atoms with isotropic displacement parameters.

CCDC-803438, -803439, -198988, -257326, -257325, -263256, -803554, -803440, -803441 and -803442 contain the supplementary crystallographic data for **1–7** and **9–11** respectively. These data can be obtained free of charge from The Cambridge Crystallographic Data Centre via www.ccdc.cam.ac.uk/data_request/cif.

Acknowledgements

Financial support from the Spanish Ministerio de Ciencia e Innovación (CTQ2007–61037 and CTQ2010–15515, FEDER supported) and the Junta de Andalucía (Proyecto de Excelencia, P07-FQM-2474) is gratefully acknowledged. This work was also supported by Ministero dell'Istruzione, dell'Università e della Ricerca (MIUR) through “Progetti di Rilevante Interesse Nazionale” (PRIN) project 2008RFEB3X “Aspetti elettronici di legame chimico, proprietà chimico-fisiche e reattività di nanocluster metallici”. We are grateful to CICA for permitting the use of their computational resources. Other computations were also carried out at the CINECA center, and the authors (A.I., C.M.) acknowledge the ISCR-CINECA HP grant HP10BNL89W.

- [1] S. Kitagawa, S. Noro in *Comprehensive Coordination Chemistry II*, Vol 7, Elsevier, Amsterdam, **2004**, p. 231.
- [2] S. L. James, *Chem. Soc. Rev.* **2003**, 32, 276.
- [3] A. K. Cheetham, C. N. R. Rao, R. K. Feller, *Chem. Commun.* **2006**, 4780.
- [4] See, for example: a) M. O'Keeffe, M. Eddaoudi, H. Li, T. Reineke, O. M. Yaghi, *J. Solid State Chem.* **2000**, 152, 3; b) A. Y. Robin, K. M. Fromm, *Coord. Chem. Rev.* **2006**, 250, 2127.
- [5] a) Y. F. Zeng, X. Hu, F. C. Liu, X. H. Bu, *Chem. Soc. Rev.* **2009**, 38, 469; b) D. Maspoch, D. Ruiz-Molina, J. Veciana, *Chem. Soc. Rev.* **2007**, 36, 770; c) M. J. Rosseinsky, *Microporous Mesoporous Mater.* **2004**, 73, 15.
- [6] Selected references are: a) B. Wang, A. P. Cote, H. Furukawa, M. O'Keeffe, O. M. Yaghi, *Nature* **2008**, 453, 207; b) T. K. Maji, R. Matsuda, S. Kitagawa, *Nat. Mater.* **2007**, 6, 142; c) L. J. Barbour, *Chem. Commun.* **2006**, 1163; d) S. Kitagawa, R. Kitaura, S. Noro, *Angew. Chem.* **2004**, 116, 2388; *Angew. Chem. Int. Ed.* **2004**, 43, 2334; e) O. M. Yaghi, M. O'Keeffe, N. W. Ockwig, H. K. Chae, M. Eddaoudi, J. Kim, *Nature* **2003**, 423, 705; f) N. L. Rosi, J. Eckert, M. Eddaoudi, D. T. Vodak, J. Kim, M. O'Keeffe, O. M. Yaghi, *Science* **2003**, 300, 1127.
- [7] See, for example: U. Mueller, M. M. Schubert, O. M. Yaghi, in *Handbook of Heterogeneous Catalysis*, Vol. 1 (Eds.: G. Ertl, H. Knözinger, F. Schüth, J. Weitkamp), Wiley, New York, **2008**, p. 247.
- [8] a) C. Janiak, *Dalton Trans.* **2003**, 2781; b) L. Brammer, *Chem. Soc. Rev.* **2004**, 33, 476.
- [9] Selected references: a) R. Q. Zou, H. Sakurai, S. Han, R. Q. Zhong, Q. Xu, *J. Am. Chem. Soc.* **2007**, 129, 8402; b) X. J. Kong, Y. P. Ren, L. S. Long, Z. P. Zheng, R. B. Huang, L. S. Zheng, *J. Am. Chem. Soc.* **2007**, 129, 7016; c) S. Kitagawa, K. Uemura, *Chem. Soc. Rev.* **2005**, 34, 109; d) J. Mrozinski, *Coord. Chem. Rev.* **2005**, 249, 2534; e) S. Kitagawa, R. Kitaura, S.-I. Noro, *Angew. Chem.* **2004**, 116, 2388; *Angew. Chem. Int. Ed.* **2004**, 43, 2334; f) R. Kitaura, S. Kitagawa, Y. Kubota, T. C. Kobayashi, K. Kindo, Y. Mita, A. Matsuo, M. Kobayashi, H. C. Chang, T. C. Ozawa, M. Suzuki, M. Sakata, M. Takata, *Science* **2002**, 298, 2358; g) M. Verdaguer, *Science* **1996**, 272, 698.
- [10] Selected references: a) G. Férey, C. Mellot-Draznieks, C. Serre, F. Millange, J. Dutour, S. Surblé, I. Margiolaki, *Science* **2005**, 309, 2040; b) H. Chun, D. N. Dybtsev, H. Kim, K. Kim, *Chem. Eur. J.* **2005**, 11, 3521; c) D. Bradshaw, T. J. Prior, E. J. Cussen, J. B. Claridge, M. J. Rosseinsky, *J. Am. Chem. Soc.* **2004**, 126, 6106; d) H. K. Chae, D. Y. Siberio-Pérez, J. Kim, Y. Go, M. Eddaoudi, A. J. Matzger, M. O'Keeffe, O. M. Yaghi, *Nature* **2004**, 427, 523; e) B. Moulton, H. Abourahma, M. W. Bradner, J. Lu, G. J. McManus, M. J. Zaworotko, *Chem. Commun.* **2003**, 1342; f) M. Eddaoudi, J. Kim, N. Rosi, D. Vodak, J. Wachter, M. O'Keeffe, O. M. Yaghi, *Science* **2002**, 295, 469; g) S. S. Y. Chui, S. M. F. Lo, J. P. H. Charmant, A. G. Orpen, I. D. Williams, *Science* **1999**, 283, 1148.
- [11] a) R. M. Wang, J. Zhang, L. J. Li, *Inorg. Chem.* **2009**, 48, 7194; b) L. Zhang, J. Zhang, Z. J. Li, Y. Y. Qin, Q. P. Lin, Y. G. Yao, *Chem. Eur. J.* **2009**, 15, 989; c) S. M. Hawxwell, G. Minguez Espallargas, D. Bradshaw, M. J. Rosseinsky, T. J. Prior, A. J. Florence, J. van de Sreek, L. Brammer, *Chem. Commun.* **2007**, 1532; d) S. M. Humphrey, P. T. Wood, *J. Am. Chem. Soc.* **2004**, 126, 13236; e) M. Sanelme, J. M. Grenèche, M. Riou-Cavellec, G. Férey, *Chem. Commun.* **2002**, 2172; f) B. Notash, N. Safari, H. R. Khavasi, *Inorg. Chem.* **2010**, 49, 11415.
- [12] See references in: a) L. Álvarez, A. Grirrane, R. Moyano, E. Álvarez, A. Pastor, A. Galindo, *Polyhedron* **2010**, 29, 3028; b) A. Grirrane, A. Pastor, E. Álvarez, C. Mealli, A. Ienco, P. Rosa, A. Galindo, *Eur. J. Inorg. Chem.* **2007**, 3543; c) D. del Río, A. Galindo, R. Vicente, C. Mealli, A. Ienco, D. Masi, *Dalton Trans.* **2003**, 1813; d) A. Grirrane, A. Pastor, E. Álvarez, C. Mealli, A. Ienco, D. Masi, A. Galindo, *Inorg. Chem. Commun.* **2005**, 8, 463; e) A. Grirrane, A. Pastor, E. Álvarez, R. Moyano, A. Galindo, *Inorg. Chem. Commun.* **2007**, 10, 1125; f) A. Grirrane, A. Pastor, A. Ienco, C. Mealli, A. Galindo, *J. Chem. Soc. Dalton Trans.* **2002**, 3771.
- [13] a) Y. Wang, M. Fang, Y. Li, J. Liang, W. Shi, J. Chen, P. Cheng, *Int. J. Hydrogen Energy* **2010**, 35, 8166; b) Y. Wang, Z.-J. Zhang, W. Shi, P. Cheng, D.-Z. Liao, S.-P. Yan, *CrystEngComm* **2010**, 12, 1086; c) T. K. Prasad, M. V. Rajasekharan, J.-P. Costes, *Angew. Chem.* **2007**, 119, 2909; *Angew. Chem. Int. Ed.* **2007**, 46, 2851; d) Y. Wang, P. Cheng, J. Chen, D.-Z. Liao, S.-P. Yan, *Inorg. Chem.* **2007**, 46, 4530.
- [14] A. Grirrane, A. Pastor, E. Álvarez, C. Mealli, A. Ienco, P. Rosa, F. Montilla, A. Galindo, *Eur. J. Inorg. Chem.* **2004**, 707.
- [15] a) A. Grirrane, A. Pastor, A. Galindo, A. Ienco, C. Mealli, P. Rosa, *Chem. Commun.* **2003**, 512; b) A. Grirrane, A. Pastor, A. Galindo, D. del Río, A. Orlandini, C. Mealli, A. Ienco, A. Caneschi, J. Fernández Sanz, *Angew. Chem.* **2005**, 117, 3495; *Angew. Chem. Int. Ed.* **2005**, 44, 3429.
- [16] H. R. Khavasi, M. Azizpoor Fard, *Cryst. Growth Des.* **2010**, 10, 1892.
- [17] H. Ramsis, E. Perez-Ruiz, J. Roger, E. Bourret, J. L. Delarbre, L. Maury, *J. Raman Spectrosc.* **1995**, 26, 131.
- [18] S. H. Whitlow, *Acta Crystallogr. Sect. B* **1975**, 31, 2531.
- [19] M.-C. Wu, C.-S. Lee, *Inorg. Chem.* **2006**, 45, 9634.
- [20] Cambridge Structural Database (CSD), Cambridge Crystallographic data Centre, 12 Union Road, Cambridge, CB2 1EZ, UK. CSD Version 5.31, Conquest 1.12 & Vista 2.1. <http://www.ccdc.cam.ac.uk/>.

- Bond length statistics were analyzed using the program Vista from a ConQuest search.
- [21] J. Delaunay, C. Kappenstein, R. P. Hugel, *J. Chem. Res.* **1978**, 48, 801.
- [22] M. G. B. Drew, D. A. Rice, C. W. Timewell, *J. Chem. Soc. Dalton Trans.* **1975**, 144.
- [23] A. Grirrane, A. Pastor, E. Álvarez, A. Galindo, *Inorg. Chem. Commun.* **2005**, 8, 453.
- [24] A. Grirrane, A. Pastor, E. Álvarez, C. Mealli, A. Ienco, A. Galindo, *Inorg. Chem. Commun.* **2006**, 9, 160.
- [25] a) S. Menage, Private communication and PhD Thesis, University of Paris Sud, Orsay (France), **1988**; b) an ORTEP diagram of $[\text{Mn}_2(\text{C}_3\text{F}_7\text{CO}_2)_4(\text{bipy})_2]$ has appeared in H. Mimoun, L. Sausine, S. Menage, J.-J. Girerd in *New Developments in Selective Oxidation* (Eds.: G. Centi, F. Trifiro), Elsevier, Amsterdam, **1990**; c) M. Nakashima, H. Maruo, T. Hata, T. Tokii, *Chem. Lett.* **1999**, 1277; d) E. V. Amel'chenkova, T. O. Desinova, S. E. Nefedov, *Mendeleev Commun.* **2004**, 14, 103; e) M. A. Kiskin, I. G. Fomina, G. G. Aleksandrov, A. A. Sidorov, V. M. Novotortsev, Y. V. Rakitin, Z. V. Dobrokhotova, V. N. Ikorskii, Y. G. Shvedenkov, I. L. Eremenko, I. I. Moiseev, *Inorg. Chem. Commun.* **2005**, 8, 89; f) L. Yang, W. Yu, T.-L. Zhang, J.-G. Zhang, S.-Z. Wang, R.-F. Wu, *Z. Anorg. Allg. Chem.* **2007**, 633, 2046; g) Z. Chen, Y. Ma, F. Liang, Z. Zhou, *Eur. J. Inorg. Chem.* **2007**, 2040; h) D.-H. Wu, J. Shi, Y.-J. Shi, G.-Q. Jiang, *Acta Crystallogr. Sect. E* **2008**, 64, m161.
- [26] See for example: *Comprehensive Coordination Chemistry*, Vol. 4 (Eds.: G. Wilkinson, R. D. Gillard, J. A. McCleverty), Pergamon Press, New York, **1987**, Chapter 1.
- [27] For other related examples, see: S.-L. Li, T. C. W. Mak, *J. Chem. Soc. Dalton Trans.* **1995**, 1519.
- [28] For a critical account on π - π stacking, see for example: C. Janiak, *J. Chem. Soc. Dalton Trans.* **2000**, 3885.
- [29] See, for example: a) B.-H. Ye, T. Mak, I. D. Williams, X.-Y. Li, *Chem. Commun.* **1997**, 1813; b) S.-B. Yu, S. J. Lippard, I. Shweky, A. Bino, *Inorg. Chem.* **1992**, 31, 3502; c) B.-H. Ye, I. D. Williams, X.-Y. Li, *J. Inorg. Biochem.* **2002**, 92, 128; d) C.-S. Liu, E. C. Sañudo, L.-F. Yan, Z. Chang, J.-J. Wang, T.-L. Hu, *Transition Met. Chem.* **2009**, 34, 51; e) A. Karmakar, K. Bania, A. M. Baruah, J. B. Baruah, *Inorg. Chem. Commun.* **2007**, 10, 959.
- [30] For a review on this subject, see: A. J. Wu, J. E. Penner-Hahn, V. L. Pecoraro, *Chem. Rev.* **2004**, 104, 903.
- [31] a) B.-H. Ye, M.-L. Tong, X.-M. Chen, *Coord. Chem. Rev.* **2005**, 249, 545; b) A. Bellucci, A. Crispini, D. Pucci, E. I. Szerb, M. Ghedini, *Cryst. Growth Des.* **2008**, 8, 3114.
- [32] a) L. F. Lindoy, I. Atkinson, *Self-Assembly in Supramolecular Systems*, RSC: Cambridge, **2000**; b) M. Kato, K. Kojima, T. Okamura, H. Yamamoto, T. Yamamura, N. Ueyama, *Inorg. Chem.* **2005**, 44, 4037; c) I. Kobrsi, J. E. Knox, M. J. Heeg, H. B. Schlegel, C. H. Winter, *Inorg. Chem.* **2005**, 44, 4894; d) A. K. Ghosh, D. Ghoshal, E. Zangrando, J. Ribas, N. Ray Chaudhuri, *Inorg. Chem.* **2005**, 44, 1786; e) D. Ghoshal, A. K. Ghosh, J. Ribas, G. Mostafa, N. Ray Chaudhuri, *CrystEngComm* **2005**, 7, 616; f) F. Zordan, S. L. Purver, H. Adams, L. Brammer, *CrystEngComm* **2005**, 7, 350; g) P. Smart, G. M. Espallargas, L. Brammer, *CrystEngComm* **2008**, 10, 1335.
- [33] R. van Gorkum, F. Buda, H. Kooijman, A. L. Spek, E. Bouwman, J. Reedijk, *Eur. J. Inorg. Chem.* **2005**, 2255.
- [34] J. Marek, Z. Travnicek, P. Kopel, *Acta Crystallogr. Sect. C* **2003**, 59, m429.
- [35] R. Baggio, M. T. Garland, J. Manzur, O. Peña, M. Perec, E. Spodine, A. Vega, *Inorg. Chim. Acta* **1999**, 286, 74.
- [36] P. Kopel, Z. Travnicek, J. Marek, J. Mrozinski, *Polyhedron* **2004**, 23, 1573.
- [37] R. P. Bonomo, E. Rizzarelli, N. Bresciani-Pahor, G. Nardin, *J. Chem. Soc. Dalton Trans.* **1982**, 681.
- [38] Selected references: a) A. Majumder, C. R. Choudhury, S. Mitra, C. Marschner, J. Baumgartner, *Z. Naturforsch. B* **2005**, 60, 99; b) G.-Y. Hsu, P. Misra, S.-C. Cheng, H.-H. Wei, S. Mohanta, *Polyhedron* **2006**, 25, 3393; c) M. E. D. de Vitar, S. Baggio, M. T. Garland, R. Baggio, *Acta Crystallogr. Sect. E* **2006**, 62, m141; d) A. Majumder, G. Pilet, M. T. G. Rodriguez, S. Mitra, *Polyhedron* **2006**, 25, 2550; e) X.-P. Sun, W. Gu, X. Liu, *Acta Crystallogr. Sect. E* **2007**, 63, m1027.
- [39] B. Wenzel, P. Lonnecke, E. Hey-Hawkins, *Organometallics* **2002**, 21, 2070.
- [40] H. Ikura, T. Nagata, *Inorg. Chem.* **1998**, 37, 4702.
- [41] See, for example, on octahedral Mn^{II} complexes with $|D|$ up to 1 cm^{-1} : C. Duboc, T. Phoeung, S. Zein, J. Pécaut, M.-N. Collomb, F. Neese, *Inorg. Chem.* **2007**, 46, 4905.
- [42] a) G. L. Abbati, L.-C. Brunel, H. Casalta, A. Cornia, A. C. Fabretti, D. Gatteschi, A. K. Hassan, A. G. M. Jansen, A. L. Maniero, L. Pardi, C. Paulsen, U. Segre, *Chem. Eur. J.* **2001**, 7, 1796; b) P. ter Heerdt, M. Stefan, E. Goovaerts, A. Caneschi, A. Cornia, *J. Magn. Reson.* **2006**, 179, 29; c) S. Blanchard, G. Blain, E. Rivière, M. Nierlich, G. Blondin, *Chem. Eur. J.* **2003**, 9, 4260; d) S. Blanchard, G. Blondin, E. Rivière, M. Nierlich, J.-J. Girerd, *Inorg. Chem.* **2003**, 42, 4568.
- [43] Figure S14 in the Supporting Information compares the 190 GHz spectra at 5 K for pellets made from powder and crushed single crystals. It can be seen that, though the features around $g=2$ decrease in intensity, they do not disappear completely. Since powder microanalysis agrees nicely with theoretical results, it is rather likely that some uncoupled Mn^{II} species is present in relatively higher concentration in the powder due to defects.
- [44] A. Bencini, D. Gatteschi, *EPR of Exchange Coupled Systems*, Springer Berlin, **1990**.
- [45] H. W. Roesky, M. Andruh, *Coord. Chem. Rev.* **2003**, 236, 91.
- [46] a) A. D. Becke, *Phys. Rev. A* **1988**, 38, 3098; b) J. O. Perdew, *Phys. Rev. B* **1986**, 33, 8822.
- [47] Gaussian 98, Revision A.7, M. J. Frisch, G. W. Trucks, H. B. Schlegel, G. E. Scuseria, M. A. Robb, J. R. Cheeseman, V. G. Zakrzewski, J. A. Montgomery, Jr., R. E. Stratmann, J. C. Burant, S. Dapprich, J. M. Millam, A. D. Daniels, K. N. Kudin, M. C. Strain, O. Farkas, J. Tomasi, V. Barone, M. Cossi, R. Cammi, B. Mennucci, C. Pomelli, C. Adamo, S. Clifford, J. Ochterski, G. A. Petersson, P. Y. Ayala, Q. Cui, K. Morokuma, D. K. Malick, A. D. Rabuck, K. Raghavachari, J. B. Foresman, J. Cioslowski, J. V. Ortiz, A. G. Baboul, B. B. Stefanov, G. Liu, A. Liashenko, P. Piskorz, I. Komaromi, R. Gomperts, R. L. Martin, D. J. Fox, T. Keith, M. A. Al-Laham, C. Y. Peng, A. Nanayakkara, C. Gonzalez, M. Challacombe, P. M. W. Gill, B. Johnson, W. Chen, M. W. Wong, J. L. Andres, M. Head-Gordon, E. S. Replogle, J. A. Pople, Gaussian Inc., Pittsburgh PA, **1998**.
- [48] C. J. O'Connor, *Prog. Inorg. Chem.* **1982**, 29, 203.
- [49] a) J. J. Borrás-Almenar, J. M. Clemente-Juan, E. Coronado, B. S. Tsukerblat, *Inorg. Chem.* **1999**, 38, 6081; b) J. J. Borrás-Almenar, J. M. Clemente-Juan, E. Coronado, B. S. Tsukerblat, *J. Comput. Chem.* **2001**, 22, 985.
- [50] a) F. Muller, M. A. Hopkins, N. Coron, M. Grynberg, L. C. Brunel, G. Martínez, *Rev. Sci. Instrum.* **1989**, 60, 3681; b) A.-L. Barra, *Appl. Magn. Reson.* **2001**, 21, 619.
- [51] a) C. J. H. Jacobsen, E. Pedersen, J. Villadsen, H. Weihe, *Inorg. Chem.* **1993**, 32, 1216; b) S. Mossin, H. Weihe, A.-L. Barra, *J. Am. Chem. Soc.* **2002**, 124, 8764.
- [52] a) P. E. Werner, L. Eriksson, M. C. Westdahl, *J. Appl. Crystallogr.* **1985**, 18, 367; L. Eriksson, M. C. Westdahl, *J. Appl. Crystallogr.* **1985**, 18, 367; b) A. Altomare, C. Giacovazzo, A. Guagliardi, A. G. G. Moliterni, R. Rizzi, P. E. Werner, *J. Appl. Crystallogr.* **2000**, 33, 1180.
- [53] A. Altomare, M. Camalli, C. Cuocci, C. Giacovazzo, A. Moliterni, R. Rizzi, *J. Appl. Crystallogr.* **2009**, 42, 1197.
- [54] A. C. Larson, R. B. von Dreele, *Generalized Crystal Structure Analysis System*, Los Alamos National Laboratory, Los Alamos, **2001**.
- [55] P. W. R. Corfield, R. J. Doedens, J. A. Ibers, *Inorg. Chem.* **1967**, 6, 197.
- [56] a) S. Parkin, B. Moezzi, H. Hope, *J. Appl. Crystallogr.* **1995**, 28, 53; b) A. C. T. North, D. C. Phillips, F. S. Mathews, *Acta Crystallogr. Sect. A* **1968**, 24, 351.
- [57] A. J. C. Wilson, *International Tables for X-Ray Crystallography*, Vol. C, Kluwer Academic Publishers, Dordrecht, **1992**, p. 500.

- [58] A. J. C. Wilson, *International Tables for X-Ray Crystallography*, Vol. C, Kluwer Academic Publishers, Dordrecht, **1992**, p. 219.
- [59] A. Altomare, M. C. Burla, M. Camalli, G. L. Cascarano, C. Giacovazzo, A. Guagliardi, A. G. C. Moliterni, G. Polidori, G. R. Spagna, *J. Appl. Crystallogr.* **1999**, 32, 115.
- [60] G. M. Sheldrick, *Acta Crystallogr. Sect. A* **2008**, 64, 112.
- [61] L. J. Farrugia, *J. Appl. Crystallogr.* **1999**, 32, 837.
- [62] ORTEP-III, M. N. Burnett, C. K. Johnson, Oak Ridge National Laboratory, Oak Ridge, **1996**.
- [63] SAINT, 6.02, BRUKER-AXS, Inc., Madison, WI, **1997–1999**.
- [64] SADABS, G. M. Sheldrick, Bruker AXS, Inc., Madison, WI, **1999**.
- [65] SIR2002; M. C. Burla, M. Camalli, B. Carrozzini, G. L. Cascarano, C. Giacovazzo, G. Polidori, R. Spagna, *J. Appl. Crystallogr.* **2003**, 36, 1103.
- [66] SHELXTL, 6.14; Bruker AXS, Inc., Madison, WI, **2000–2003**.

Received: March 31, 2011

Please note: Minor changes have been made to this manuscript since its publication in *Chemistry—A European Journal* Early View. The Editor.

Published online: August 10, 2011